

Selective Activation of AMPK β 1-containing Isoforms Improves Kidney Function in a Rat Model of Diabetic Nephropathy

Christopher T Salatto, Russell A Miller, Kimberly O Cameron, Emily Cokorinos, Allan Reyes,
Jessica Ward, Matt Calabrese, Ravi Kurumbail, Francis Rajamohan, Amit S Kalgutkar, David A.
Tess, Andre Shavnya, Nathan E Genung, David J Edmonds, Aditi Jatkar, Benjamin S
Maciejewski, Marina Amaro, Harmeet Gandhok, Mara Monetti, Katherine Cialdea, Eliza
Bollinger, John M Kreeger, Timothy M Coskran, Alan C Opsahl, Germaine G Boucher, Morris J
Birnbaum, Paul DaSilva-Jardine and Tim Rolph

CVMET Research Unit, Pfizer Worldwide Research and Development, Cambridge, MA 02139
(CS, RM, EC, AR, JW, AJ, BM, MA, HG, MM, KC, EB, MB, PD, TR)

Worldwide Medicinal Chemistry, Pfizer Worldwide Research and Development, Cambridge, MA
02139 (KC, DE)

Worldwide Medicinal Chemistry, Pfizer Worldwide Research and Development, Groton, CT
06340 (MC, RK, FR, AS, NG)

Pharmacokinetics, Dynamics, & Metabolism, Pfizer Worldwide Research and Development,
Cambridge, MA 02139 (AK, DT)

Drug Safety Research and Development, Pfizer Worldwide Research and Development, Groton,
CT 06340 (JK, TC, AO, GB)

Co-corresponding authors (CS, RM)

JPET #237925

Running Title: Activation of AMPK β 1 Improves Rodent Kidney Function

Correspondence addressed to:

Christopher T Salatto
Pfizer Worldwide Research and Development
235 East 42nd Street
New York, NY 10017
(212)-733-7925
christopher.t.salatto@pfizer.com

or

Russell A Miller
Pfizer Worldwide Research and Development
1 Portland Street
Cambridge, MA 02139
(617)-551-3260
Russell.miller@pfizer.com

Text Pages: 28
Tables: 1
Figures: 6
Abstract: 187 words
Introduction: 398 words
Discussion: 403
References: 24

Non-standard abbreviations:

ACC: Acetyl-CoA carboxylase
ACEi: Angiotensin Converting Enzyme inhibitor
AMPK: Adenosine Monophosphate-activated Protein Kinase
PGC1 α : Peroxisome proliferator-activated receptor- γ coactivator-1 α
PRKAB1: Protein Kinase AMP-Activated Non-Catalytic Subunit Beta 1
TBC1D1: TBC1 domain family member 1
TIMP1: Tissue Inhibitor of Metalloproteinases 1
TSC2: Tuberous Sclerosis Complex 2
TBAR: Thiobarbituric Acid Reactive Substance

Section assignment:

- 1) Drug Discovery and Translational Medicine
- 2) Gastrointestinal, Hepatic, Pulmonary, Renal

Conflict of Interest Statement

All authors were employees of Pfizer Inc. at the time these experiments were conducted.

Abstract

Diabetic nephropathy remains an area of high unmet medical need, with current therapies that slow down, but do not prevent the progression of disease. A reduced phosphorylation state of adenosine monophosphate-activated protein kinase (AMPK) has been correlated with diminished kidney function in both humans and animal models of renal disease. Here, we describe the identification of novel, potent, small molecule activators of AMPK that selectively activate AMPK heterotrimers containing the $\beta 1$ subunit. After confirming that human and rodent kidney predominately express AMPK $\beta 1$, we explore the effects of pharmacological activation of AMPK in the ZSF1 rat model of diabetic nephropathy. Chronic administration of these direct activators elevate the phosphorylation of AMPK in the kidney, without impacting blood glucose levels, and reduce the progression of proteinuria to a greater degree than the current standard of care ACE-inhibitor ramipril. Further analyses of urine biomarkers and kidney tissue gene expression reveal AMPK activation leads to the modulation of multiple pathways implicated in kidney injury, including cellular hypertrophy, fibrosis, and oxidative stress. These results support the need for further investigation into the potential beneficial effects of AMPK activation in kidney disease.

Introduction

The incidence of the metabolic syndrome is rising across the world, presenting patients and society with an increasing need for transformative therapies to treat this cluster of co-morbidities. Patients who suffer from Diabetic Nephropathy (DN), a form of chronic kidney disease that is linked mechanistically to diabetes and the metabolic syndrome, are in acute need of disease modifying treatment options that will delay or prevent the progression to end stage renal disease (Gallagher and Suckling, 2016). The etiology of this disease progression is complex because of an interplay between systemic metabolic and vascular dysfunctions that involves both tubular and glomerular renal systems; this has made the rational identification of novel disease modifying therapeutic targets difficult (Vallon and Komers, 2011). We have chosen to focus on targets where there is a concordance between genetic loci associated with disease and evidence of efficacy in preclinical models; one potential therapeutic target that satisfies these two criteria is the protein kinase, adenosine monophosphate-activated protein kinase (AMPK) (Hallows et al., 2010; Kottgen et al., 2010).

AMPK is a heterotrimeric kinase that is activated by changes in cellular energy levels, leading to phosphorylation of its target proteins, which include Acetyl-CoA carboxylase, TSC2, Raptor, TBC1D1, and PGC1 α , resulting in increased energy production and reduced energy consumption (Mihaylova and Shaw, 2011). AMPK has been studied in many organ systems and has been actively pursued as a therapeutic target for metabolic syndrome, in part because of the observation that elevated nutrient status results in low AMPK activity (Steinberg and Kemp, 2009). Reduced phosphorylation of the AMPK α subunit at the activating threonine 172 site has been observed in renal glomeruli of diabetic patients, suggesting that low AMPK activity in the diabetic state could be part of the etiology of DN progression (Dugan et al., 2013). Multiple interventional studies in rodent models of diabetic kidney disease have suggested the potential benefits of activating AMPK for DN. Many of these studies utilized activators of AMPK

JPET #237925

that also have AMPK-independent activities, which could impact kidney function autonomously or non-autonomously and are limited in their capacity to activate AMPK at clinically relevant doses (Lee et al., 2007; Sharma et al., 2008; Dugan et al., 2013; Kim et al., 2013; Yuan et al., 2014). We therefore set out to identify novel, specific, small molecule activators of AMPK that hold the potential for clinical development as a treatment option for Diabetic Nephropathy (DN).

Materials and Methods

TR-FRET Protection-Activation Assay

AMPK allosteric activation and/or protection from dephosphorylation was determined using a novel two step TR-FRET kinase assay designed to measure both changes in intrinsic activity (activation) and phosphorylation at Thr172 of the α -subunit (protection). The first step of the assay involves treatment with a phosphatase to dephosphorylate pAMPK by approximately 50%. This condition was chosen since it reduced the population of pAMPK sufficiently to generate an acceptable protection assay window, while preserving enough pAMPK to measure activity and allosteric activation. Following the dephosphorylation step, the remaining phosphatase activity was terminated with okadaic acid and kinase activity was monitored using a TR-FRET assay format as previously described utilizing a Cy5 labeled SAMS peptide and a Europium labeled phospho-ACC (Ser79) mouse monoclonal antibody (Calabrese et al., 2014).

All assays were performed in 384-well low volume white opaque plates (Corning, New York, NY) with a 20 μ L total reaction volume. Reactions were carried out in assay buffer containing 50 mM HEPES, pH 7.5, 1 mM EGTA, 10 mM $MgCl_2$, 0.25 mM DTT, 0.01 % Tween-20 and 0.01% BSA. Compound was tested at 11 different doses against human AMPK $\alpha 1\beta 1\gamma 1$, rat AMPK $\alpha 1\beta 1\gamma 1$, human AMPK $\alpha 1\beta 2\gamma 1$, human AMPK $\alpha 2\beta 1\gamma 1$, human AMPK $\alpha 2\beta 2\gamma 1$ and human AMPK $\alpha 2\beta 2\gamma 3$. All assays were performed with 50 nM Cy5 labeled SAMS peptide and ATP concentration equal to the K_m for each isoform. (20uM, 20uM, 40uM, 20uM, 40uM, 100uM final for AMPK $\alpha 1\beta 1\gamma 1$, rat AMPK $\alpha 1\beta 1\gamma 1$, human AMPK $\alpha 1\beta 2\gamma 1$, human AMPK $\alpha 2\beta 1\gamma 1$, human AMPK $\alpha 2\beta 2\gamma 1$ and human AMPK $\alpha 2\beta 2\gamma 3$ respectively).

Compound was serially diluted in 100% dimethyl sulfoxide (DMSO) and 1 μ L was spotted in duplicate into a compound plate. For each compound plate, corresponding positive control wells (40 μ M AMP) and negative control wells (DMSO) were also added. The compounds were

then diluted to 8% DMSO in buffer and five μ L was transferred to a white assay plate. To this mixture, five μ L of AMPK enzyme diluted in assay buffer was added to the assay plate (0.25nM, 0.25nM, 0.5nM, 2nM, 1nM, 1nM final for human AMPK α 1 β 1 γ 1, rat AMPK α 1 β 1 γ 1, human AMPK α 1 β 2 γ 1, human AMPK α 2 β 1 γ 1, human AMPK α 2 β 2 γ 1 and human AMPK α 2 β 2 γ 3 respectively) and incubated at room temperature for 15 minutes. Next, five μ L of PP2a (2.5nM, 2.5nM, 5.0nM, 0.25nM, 0.25nM, 0.25nM final for AMPK α 1 β 1 γ 1, rat AMPK α 1 β 1 γ 1, human AMPK α 1 β 2 γ 1, human AMPK α 2 β 1 γ 1, human AMPK α 2 β 2 γ 1 and human AMPK α 2 β 2 γ 3 respectively) diluted in assay buffer was added and the plate was incubated for an additional 60 minutes. PP2a was selected not only for its activity against pAMPK, but also for its ability to be inhibited by okadaic acid, a potent inhibitor that does not interfere with the assay technology. The phosphatase treatment was terminated and the kinase reaction initiated with the addition of 5 μ L of okadaic acid (50nM final, Calbiochem, San Diego, CA), Cy5-SAMS peptide and ATP diluted in assay buffer. The kinase reactions were incubated for 60 min at room temperature and terminated by the addition of 10mM EDTA and 2 nM Eu-pACC antibody in LANCE Detection Buffer (Perkin Elmer, Waltham, MA). Kinase activity was monitored by excitation at 320 nm and measuring emission at 665 and 615 nm, respectively using EnVision® multilabel reader (Perkin Elmer) in TR-FRET mode. The final ratio of fluorescence emissions at wavelengths 665/615 nm (emission from phosphorylated SAMS peptide/emission from the europium antibody) was used to calculate the percent effect relative to the AMP and DMSO controls. The percent effect values were then plotted against the concentrations of compound and the EC₅₀ values were calculated using GraphPad prism software.

Protection Assay

The ability of AMPK activators to protect pAMPK from dephosphorylation was determined using Dissociation-Enhanced Lanthanide Fluorescent Immunoassay technology (DELFI®). Briefly,

test compounds were incubated with fully phosphorylated biotin acceptor peptide (BAP)-tagged AMPK in assay buffer consisting of 50 mM HEPES, pH 7.5, 1 mM EGTA, 10 mM MgCl₂, 0.25 mM DTT, 0.01 % Tween-20 and 0.01% BSA. PP2a was then added to the mixture and allowed to proceed for 60 min at room temperature to dephosphorylate the AMPK protein by about 70%. Reactions were terminated by the addition of okadaic acid and the mixture was transferred to a DELFIA® streptavidin-coated 384 well white plate and allowed to incubate with gentle shaking for 1 hour at room temperature. Wells were washed 6 times and captured AMPK was probed with primary anti- α subunit-pThr172 antibody for 45 min with gentle shaking at room temperature, and then washed 5 times as above. Wells were probed with DELFIA® Eu-N1 labeled anti-rabbit antibody for 45 min with gentle shaking and washed as above. The signal was developed by the addition of DELFIA® enhancement solution and time-resolved fluorescence was measured using an EnVISION™ plate reader (PerkinElmer) with the factory-set DELFIA® europium protocol (excitation at 340 nm and emission at 615 nm).

Determination of the mechanism of activation

Steady state kinetic experiments to determine the mechanism of allosteric activation of the compounds were performed by monitoring incorporation of ³³P-phosphate from ³³P-ATP into the SAMS peptide substrate as previously described (Calabrese et al., 2014; Rajamohan et al., 2015).

Crystallization and Refinement:

The $\alpha 1\beta 1\gamma 1$ crystallization construct of rat AMPK was expressed and purified as previously described with the exception of a single mutation of Asn109 in the $\beta 1$ subunit to His as is found in the human protein (Calabrese et al., 2014). His109 lies in the vicinity of the allosteric binding site, but the limited resolution of the X-ray diffraction data do not permit detailed analysis of the subtle differences in the structure caused by this mutation. Lysine 29 of the alpha subunit is

modeled in a conformation similar to previous observations although electron density is not well-defined for the side chain.

Crystallization was carried out by sitting drop vapor diffusion by mixing equal volumes of protein (~11 mg/mL) and precipitant. Crystallization conditions consisted of a grid around the base condition of 100 mM trisodium citrate, 500 mM ammonium sulfate, 900 mM lithium sulfate, and 4% glycerol. Crystals grew over the course of 3-10 days at approximately room temperature.

In order to determine the structure with PF-249, crystals were soaked overnight in mother liquor supplemented with 400 μ M AMP, 400 μ M Staurosporine, and 500 μ M PF-249 with 10% glycerol. For cryoprotection, crystals were transferred to an identical solution containing 28% glycerol. Data was collected at the IMCA-CAT beamline at APS and were processed using HKL2000 (Otinowski and Minor, 1997). Structure was solved by molecular replacement using our previous structure (4QFR) as a search model. Refinement and rebuilding were carried out using autoBUSTER and Coot and figures were generated using PyMOL (Schrodinger) (Blanc et al., 2004; Emsley and Cowtan, 2004). Nucleotides on the gamma subunit were modeled as previously described and subject to the same caveats (Calabrese et al., 2014).

Quantification of β 1 AMPK

Kidney samples were collected from C57Bl6J mice (Jackson Labs), Wistar-han rats (Charles River), and cynomolgus non-human primates, and post-mortem human (Analytical Biological Services, Inc). The rodent tissue samples were immediately snap-frozen in liquid nitrogen. Primate samples were collected during necropsy and frozen on dry ice. Human kidney samples were acquired in collaboration with the Cleveland Clinic (Cleveland, OH), and Cornell University (Ithaca, NY). The amount of β 1 and β 2 AMPK was quantified using a modified version of the ThermoFisher Scientific AMPK Phospho-ELISA Kit. Kidney lysate from three species was added to the microwells of two plates pre-coated with an AMPK α mouse antibody.

Recombinant human $\alpha 1\beta 1\gamma 1$ AMPK was used as a standard curve on one plate. To detect $\beta 1$ AMPK, rabbit anti-AMPK $\beta 1$ (4 ug/mL) was added to each well. On the second plate, recombinant human $\alpha 2\beta 2\gamma 1$ was used as a standard curve. To detect $\beta 2$ AMPK, rabbit anti-AMPK $\beta 2$ (4 ug/mL) was added to each well. Anti-rabbit IgG, HRP-linked antibody was then used to recognize the bound detection antibody. HRP substrate, TMB, was added to develop color. The magnitude of the absorbance was measured at 450 nm. The standard curve was plotted for each plate and data were interpolated to the $\beta 1$ or $\beta 2$ standard curves, respectively, using SoftMax Pro. Picomolar per gram total protein values were calculated for the $\beta 1$ isoform in Excel, as well as the relative percent of $\beta 1$ versus $\beta 2$.

in vitro knockdown of pACC/tACC

293FT cells were grown in DMEM prepared with 10% FBS, 1 mM sodium pyruvate, 0.1 mM non-essential amino acids, 6 mM L-glutamine and 1% penicillin-streptomycin. siRNA duplexes purchased from Life Technologies (s11060 for *PRKAB1* knockdown, and negative control #1 catalogue number 4390843) were complexed with RNA-max as described in the manufacturer protocol. Control and *PRKAB1* siRNA were added to cells and incubated overnight. After 48 hours, cells were serum starved in Opti-MEM Reduced Serum Medium for two hours. PF-249 and PF-06409577 were prepared in DMSO and cells were treated with a final concentration of 1 μ M and 3 μ M with 0.1% final DMSO concentration. Cells pre-treated with both the control-scrambled siRNA and the *PRKAB1* siRNA were dosed with either DMSO or compound. After 1 hour, cells were rinsed with PBS and lysed in ice-cold lysis buffer. Protein content was quantified by a bicinchoninic acid (BCA) based protein assay.

Lysate was prepared for western blot analysis by adding reducing agent and lithium dodecyl sulfate and boiling for 10 minutes. Samples were loaded onto two identical Bis-Tris gel and run at 200 volts for 60 minutes. BisTris gels were blotted on to a nitrocellulose membrane for 60 minutes at 30 volts, following a standard wet transfer protocol. Membranes were blocked in 5%

non-fat milk prepared in Tris-Buffered Saline (TBS). After one hour, membranes were washed and antibody prepared in 5% Bovine Serum Albumin prepared in TBS with 0.1% Tween-20. Rabbit anti-Pan α AMPK antibody and Rabbit anti- β 1 and β 2 AMPK antibody were incubated overnight at 4°C. Membranes were washed and incubated with Anti-Rabbit IgG, HRP-linked antibody diluted in 5% non-fat milk in TBS. After one hour, membranes were washed, enhanced chemiluminescent substrate was added, and membranes were developed in bright-field white light.

Cell culture and siRNA treatment was repeated. Protein content was quantified. Phosphorylated (Serine 79) ACC and total ACC protein levels were quantified using two electrochemiluminescent immunoassay based on the technologies provided by Meso Scale Discovery (Rockville, MD). Cell lysates were added to streptavidin coated plates and incubated for 2 hours at 37°C. To detect phosphorylated (Ser79) ACC or total ACC levels, Anti-phosphoACC (Ser79) Rabbit polyclonal antibody (Millipore #07-303, at 2 μ g/mL) or Anti-ACC Rabbit monoclonal antibody (Cell Signaling Technologies #3676, at 1 mg/mL) were use, respectively. SULFO-TAG™ labeled Goat Anti-Rabbit antibody was then used to recognize the bound detection antibody. MSD Read Buffer was added to initial the electrochemiluminescent reaction. The magnitude of the luminescence was measured using the SECTOR S600 plate reader.

ZSF1 Rat Studies

All animal experiments were conducted following study protocols and procedures reviewed and approved by Pfizer Institutional Animal Care and Use Committee. The facilities that supported this work are fully accredited by AAALAC International. For each study, six week-old, male ZSF1 lean and ZSF1 obese rats (Charles River, Wilmington, MA) were acclimated to the vivarium for 14 days prior to measurement of body weight and baseline evaluation of urine. Six

days later, obese rats were assigned to one of five groups based upon urine albumin creatinine ratio (Siemens Advia 2400), urine protein creatinine ratio (Siemens Advia 2400), body weight, 24-hour urine albumin (Siemens Advia 2400), and urine volume (supplemental Table 4). Daily administration of 0.5% methylcellulose (p.o.), PF-06409577 at 10, 30, or 100 mg/kg (p.o.), PF-249 at 3, 10, or 30 mg/kg (p.o.), or ramipril in drinking water (~1 mg/kg/day) (Zoja et al., 2011) was initiated and continued for 68 days. Urine was collected for 24-hours and volume recorded from all lean and obese rats after 14, 28, 42, and 60 days of dosing. On Day 63 all rats were administered a final dose after 16-hour overnight fasting. One hour following the final dose, blood glucose was measured by glucometer (AlphaTrak 2, Zoetis) and a 100 µl tail vein blood sample collected and processed for determination of insulin levels (Alpco) and total protein (Advia 2400, Siemens). Each rat was then anesthetized with isoflurane. The right kidney was collected and immediately freeze-clamped and transferred to liquid nitrogen storage; the left kidney was fixed in 10% formalin. Rats were then euthanized by exsanguination from the vena cava.

In a separate study, blood pressure was monitored continually in 14-week old, telemeterized male, obese ZSF1 rats at were administered vehicle or PF-06409577 at 10, 30 or 100 mg/kg (p.o.) (n=10/group) for 14 days. Fifteen minute intervals of data from each animal was grouped into blocks of time, 0-2, 2-4, 4-8, 8-12, 12-16, 16-20, and 20-24 hours post dose. Statistical analysis will compare the variances of data for drug treated and vehicle animals at each time block (adjusted for baseline) using ANOVA at days 1, 6, and 14.

Kidney Gene Expression

Tissue was pulverized under frozen conditions and 30 mg lysed in 1 mL of Qiazol reagent (Qiagen, USA) using MP Biomedical Lysing Matrix D tubes. 0.2 mL of chloroform (Sigma Aldrich, USA) was added and tubes were disrupted by vortexing. Samples were then spun at

10,300 rpm at 4°C for 15 minutes to ensure phase separation. 0.2 mL of the upper aqueous phase was then placed in a gDNA eliminator column (Qiagen, USA) and eluted. The sample was mixed with 0.2 mL of fresh 70% ethanol, and the sample was added to a 96-well RNeasy plate (Qiagen, USA) vacuum system. The wash procedure included in the RNeasy kit was then followed, and the final sample was eluted in 60 mL of RNase-free water. RNA concentration and purity was evaluated using a NanoDrop ND-8000 spectrophotometer (ThermoFischer, USA). RNA was then diluted for a concentration of 100 ng per 10 µl, matched with 10 µl of High Capacity cDNA Reverse Transcriptase Kit (Applied Biosystems, USA). cDNA was then processed on a GeneAmpk PCR System 9700 according to kit directions. 400 ng of cDNA sample, Taqman primers (Applied Biosystems, USA) and TaqMan Fast Universal PCR Master Mix (Applied Biosystems, USA) was loaded onto 384-well PCR reaction plates (Applied Biosystems, USA) and run on a Viia 7 PCR system. Analysis was performed to determine reference gene outliers, and Ct values were transformed into relative quantification data. The delta Ct was generated by removing the background of the housekeeping gene from the sample of interest. Results were then generated using the comparative delta delta Ct method and were normalized to the obese vehicle treated animals. Genes were normalized to PPIa mRNA.

Urine Analysis

All urine samples were centrifuged to pellet sediment and stored at -80°C prior to analysis. Kim1/Tim1 was measured using the Quantikine RAT TIM-1/KIM-1 Immunoassay R&D Systems Cat# RKM100. Samples were diluted four fold and manufacturer's protocol followed with samples values calculated based on the provided KIM1 standards. TBAR assay was purchased from R&D Systems, Cat#KGE013, and used at a 1:2 dilution of urine according to manufacturer's protocol. TIMP1 was measured with Sigma Aldrich ELISA, cat#RAB0470, using a 20 fold dilution of urine and following the manufacturer's protocol. Creatinine, total protein,

and Albumin were measured by clinical analyzer. Urine markers measured by ELISA were corrected for daily urinary excretion by expression as the ratio with urinary creatinine.

Kidney Histology and phospho-S6 Quantification

Rat kidneys were trimmed in a coronal fashion before being immersed in 10% neutral buffered formalin (NBF). After fixation, kidneys were processed to paraffin blocks following standard tissue processing protocols. Five micron sections of kidney were sectioned using a rotary microtome and mounted on glass slides for subsequent staining. All immunohistochemistry (IHC) steps were performed on the Leica Bond III (Leica Microsystems, Buffalo Grove, IL). Briefly, slides were deparaffinized utilizing Leica's Bond dewax solution and pretreated by using Epitope Retrieval Solution #1 (Leica Microsystems) for 30 minutes with heat. Following pretreatment, non-specific binding was blocked by using Dako's serum free protein block (Dako, Carpinteria, CA). A rabbit anti human phospho S6 ribosomal protein ser235-236 monoclonal antibody (Cell Signaling Technology, Danvers, MA) was incubated at a dilution of 1/200 for 15 minutes at room temperature. Positive staining was detected by using Leica's Refine Polymer kit which includes an anti-rabbit polymer and diaminobenzidine (DAB) for visualization. All slides were counterstained with hematoxylin, dehydrated through a series of graded alcohols and xylenes, and mounted with cover slips. Additionally, a rabbit isotype control (Vector Laboratories, Burlingame, CA) was run in parallel using all the same pretreatment and detection steps.

Microscope slides with kidney sections stained for pS6 were scanned on the Leica/Aperio AT2 whole slide digital scanner at the 20X objective setting. Images were saved in .svs format and stored in Aperio eSlide Manager image database.

An image analysis rule set was created in Definiens Tissue studio that allowed for the manual outline of individual glomeruli. Manual outlines of glomeruli were sampled from three uniform

10x fields from each section At least 20 glomeruli from each section were sampled. A threshold for pS6 stain was applied to each glomerulus. A measurement of percent pS6 stain area per glomerulus was transferred to Excel. A mean pS6 stain percent area per glomerulus was calculated for each group. Statistics and graphing were completed in GraphPad Prism software.

Determination of pAMPK/tAMPK in Tissues

Frozen kidney samples were pulverized over liquid nitrogen and transferred to homogenization tubes containing ceramic beads. Ice-cold lysis buffer with protease and phosphatase inhibitors was added to each tube. Samples were secured on the FastPrep-24 benchtop tissue homogenizer and lysed at 6.5 meters/second (m/s) for 60 seconds at 4°C. The homogenate was spun in a table-top micro-centrifuge at 20,800 relative centrifugal force (rcf) for 10 minutes at 4°C. The supernatant was collected and the protein content of the lysate was measured. Lysate was stored at -80°C for future use.

pAMPK/tAMPK Assay Methods

Phosphorylated (Threonine 172) AMPK and total AMPK protein levels were quantified using a modified version of the solid phase sandwich enzyme-linked immunosorbent assay (ELISA) from Cell Signaling Technologies. Kidney tissue lysates were added to microwells pre-coated with an AMPK α rabbit antibody. Fully phosphorylated recombinant human $\alpha 2\beta 2\gamma 1$ AMPK was used as a standard curve. To detect Thr172 phosphorylation or total AMPK levels, anti-phospho AMPK (Thr172) mouse antibody or anti-AMPK β mouse antibody were used, respectively. Anti-mouse IgG, HRP-linked antibody was then used to recognize the bound detection antibody. HRP substrate, 3,3',5,5'-Tetramethylbenzidine (TMB), was added to develop color. The magnitude of the absorbance was measured at 450 nm. The standard

JPET #237925

curve was plotted and data were interpolated to the standard curve using SoftMax Pro. The ratio of phosphorylated to total AMPK protein were calculated.

Statistical Analysis

Statistics were calculated in GraphPad Prism. One way or two way Anova was performed and multiple comparison analysis done to evaluate significance between indicated groups. *

indicates $p < 0.05$, ** $p < 0.01$, *** $p < 0.001$, and **** $p < 0.0001$.

Results

PF-06409577 and PF-249 are selective activators of AMPK β 1-containing heterotrimers

Using a novel AMPK assay format to measure the activation and protection of the AMPK α 1 β 1 γ 1 heterotrimer, we determined the EC₅₀ for PF-06409577 to be 6 nM (human); 5 nM (rat), and for PF-249 to be 9 nM (human); 5 nM (rat). Both compounds were also tested against the human α 1 β 2 γ 1, α 2 β 2 γ 1, and α 2 β 2 γ 3 heterotrimers, showing weak activity for each. (Figure 1a-b). PF-06409577 and PF-249 exhibited minimal off-target pharmacology based on a broad panel of other receptors, channels, PDEs and kinases (supplemental tables 1-3 and (Cameron et al., 2016)). Both compounds activated AMPK through direct allosteric activation by reducing the K_m for peptide substrate from 28 to 6.3 μ M for PF-249, and by decreasing dephosphorylation of the activation loop Threonine 172, catalyzed by the phosphatase PP2A (Supplemental Figure 1). To further characterize protein-ligand interactions, we determined the crystal structure of PF-249 bound to the α 1 β 1 γ 1 isoform of AMPK at ~3.5 Å resolution, observing strong electron density corresponding to ligand that maps to the interface between the N-lobe of the kinase domain of the α 1 subunit and the carbohydrate binding motif of the β -subunit (Figure 1c-d).

AMPK β 1 is highly expressed in rodent and human kidney

The selectivity of the AMPK activators for β 1-containing isoforms prompted us to quantify both the total and relative expression of AMPK isoforms across several species of interest. We observed that the β 1 subunit is present in 93.1%, 95.5%, 33.3%, and 64.0% of all AMPK heterotrimers in the normal C57Bl6J mouse, Wistar Han rat, non-human primate, and human kidney, respectively. Across the four species we tested, mouse (158 pmol/g) contained the highest concentration of β 1-containing isoforms, followed by rat (128 pmol/g), human (114 pmol/g), and non-human primate (35 pmol/g). (Figure 1e)

PF-06409577 and PF-249 are selective for AMPK β 1 in cells

To confirm PF-06409577 and PF-249 could activate AMPK in intact cells and that the β 1-selectivity was preserved, experiments were performed in 293FT cells with an RNAi knockdown of the corresponding gene, *PRKAB1*. The AMPK β 1 subunit protein was significantly reduced in cells transfected with RNAi duplexes targeting *PRKAB1* mRNA (Figure 2a). Additionally, RNAi knockdown of *PRKAB1* resulted in a lowering of total AMPK α protein in addition to AMPK β 1, which is likely attributable to the high contribution of AMPK β 1 to AMPK heterotrimers in the untransfected cells. Both compounds significantly increased phosphorylation of ACC in control cells transfected with the scrambled RNA duplexes, indicative of activation of intracellular AMPK (Figure 2b-c). PF-06409577 and PF-249 exhibited reduced ACC phosphorylation in cells with reduced AMPK β 1 expression (Figure 2b-c).

Both PF-06409577 and PF-249 are orally bioavailable and dose-dependently increase the phosphorylation of AMPK in the kidney

Pharmacokinetic and pharmacodynamic properties of PF-06409577 and PF-249 were initially evaluated in male Wistar Han rats. The plasma half-lives of PF-06409577 and PF-249 were 1.06 and 27.2 h, respectively, with oral bioavailabilities ranging from 47–52% (Supplemental Table 4). Maximal doses for subsequent in vivo studies were selected by measuring kidney phosphoAMPK/total AMPK (pAMPK/tAMPK) ratios following a single, oral dose of either PF-06409577 or PF-249. Both compounds dose-dependently increased the pAMPK/tAMPK with PF-06409577 achieving a maximal response at 100 mg/kg (Cameron et al., 2016) ; PF-249 response plateaued at the 30 mg/kg dose (Supplemental Figure 2)

Activation of AMPK β 1-containing heterotrimers in a rat model of diabetic nephropathy altered the progression of proteinuria and improved urine biomarkers of kidney disease

The ZSF1 rat is a commonly used in vivo model of DN as it exhibits many characteristics of the human disease (Bilan et al., 2011; Boustany-Kari et al., 2016). We employed this model to evaluate whether direct activation of AMPK has an effect on proteinuria and the overall kidney function. Obese ZSF1 rats exhibited mild proteinuria at 8 weeks of age and progressed rapidly to more severe kidney dysfunction (Figure 3a). Oral administration of PF-06409577 (10, 30, and 100 mg/kg QD) resulted in dose-dependent reductions in proteinuria in the obese ZSF1 animals, with greater than 2-fold reduction in 24-hour urinary albumin loss compared to vehicle control after 60 days of treatment (Figure 3a). Histological assessment of the kidneys from these rats revealed a reduction in the presence of protein casts in the tubules of both PF-06409577 and ramipril treated animals, but we failed to rigorously identify improvements in glomerular structures of treated animals (Supplemental Figure 3). Additionally, administration of PF-06409577 had no significant effect on the hyperglycemia and insulin resistance displayed by all groups of obese ZSF1 rats (Figure 3c-d). Further, when the improvement in proteinuria was compared with the observed plasma drug exposure and corrected for plasma protein binding, the IC_{50} for the effect was calculated to be 5.5 nM (Supplemental figure 3, 4, and 5). Moreover, the inhibitory effect on proteinuria correlated with a dose-dependent increase in kidney pAMPK levels (Figure 3b).

We also assessed the impact of PF-06409577 on systemic blood pressure as a potential explanation for the improvement in kidney function in the ZSF1 rat in telemeterized animals. PF-06409577 delivered at 100 mg/kg had some modest reductions in systemic blood pressure at times during the day, but treatment did not cause a sustained and consistent effect (Figure 3e-f).

To replicate our initial observation, the related AMPK activator PF-249 was compared with PF-06409577 and the Angiotensin Converting Enzyme inhibitor (ACEi), ramipril, in the same model. As observed previously, progressive elevation in proteinuria in obese ZSF1 rats was attenuated

by both AMPK activators PF-06409577 and PF-249, the latter in a dose dependent manner following 68 days of dosing (Figure 4a). Modeling of the dose-dependent improvements in proteinuria observed in this study, using the observed plasma drug exposure corrected for plasma protein binding, revealed an IC_{50} for the effect of 32 nM for PF-249 and 14.5 nM for PF-06409577 (Supplemental figure 3, 6, and 7). The top dose tested for both AMPK activators resulted in a reduction of UACR, UPCR and 24-hour urinary albumin excretion equivalent to or greater than that achieved with ramipril (Figure 4a and Table 1). These improvements in urinary albumin excretion were accompanied by AMPK activation in the kidney for animals treated with AMPK activators (Figure 4b).

PF-06409577 and PF-249 improve mechanistic markers of kidney function

We explored additional endpoints to increase the understanding of the biological consequences of AMPK activation in the kidney that might account for the improvements in renal function. Urinary levels of KIM1, a marker of general tissue damage, were reduced to a similar extent, >40% ($P<0.01$), by PF-249, PF-06409577, and ramipril (Table 1). Urinary levels of TIMP1, a tissue metalloprotease inhibitor that is elevated in states of fibrosis, were elevated in obese animals with impaired kidney function and reduced ($P<0.01$) by PF-249 and PF-06409577 treatment, with the highest dose groups approaching the levels detected in lean animals with normal kidney function (Table 1). Ramipril also lowered ($P<0.05$) TIMP1, although to a lesser degree than the AMPK activators. Urinary thiobarbituric acid reactive substances (TBARs) are an indicator of reactive oxygen species (ROS)-mediated production of reactive lipid species in the setting of kidney dysfunction. As expected, the obese animals in these studies exhibited elevated urinary TBARs. Treatment with PF-249, PF-06409577, and ramipril reduced ($P<0.01$) TBARs levels towards those observed in lean animals. In aggregate, these results demonstrated improvements to multiple facets of the diseased ZSF1 kidney, while revealing subtle differences in biological responses to AMPK activators compared with ramipril.

PF-06409577 lowers glomerular mTOR signaling

Glomerular mTOR activity is an established driver of podocyte hypertrophy and compromised filtration barrier (Godel et al., 2011; Inoki et al., 2011; Inoki and Huber, 2012; Eid et al., 2013). AMPK is well-known to be negative regulator of mTORC1, raising the possibility that this mechanism could be responsible for the improvements in renal function observed in obese ZSF1 rats treated with AMPK activators. Phosphorylation state of ribosomal S6 kinase (p-S6) is a marker of mTOR activation that has been used histologically to evaluate glomerular mTOR signaling (Godel et al., 2011). Histological assessment of obese ZSF1 kidneys revealed kidneys with increased p-S6 levels within the glomeruli (Figure 5a-d), consistent with the above hypothesis. Treatment of obese ZSF1 animals with 100 mg/kg PF-06409577 reduced p-S6 within glomeruli to levels comparable to lean animals and significantly less than vehicle treated obese ZSF1 rats (Figure 5a-d).

PF-06409577 and PF-249 impact kidney mRNA of mechanistic markers

To gain further insight into the mechanism(s) underlying the improvement in kidney function upon AMPK activation, mRNA expression was also evaluated in kidney tissue samples from the chronically treated ZSF1 rats. The potential of AMPK activation to modify fibrosis was assessed by exploring the expression of the *Col1a1* and *Col4a1* mRNAs that encode the major collagens. Both transcripts were elevated in diseased animals, with PF-249 and PF-06409577 treatment reducing *Col1a1* ($P<0.01$) but not *Col4a1* expression (Figure 6a-b). It has been reported that AMPK activation reduces levels of the NADPH-oxidase Nox4 and this may be responsible for improvement of kidney function (Sharma et al., 2008; Eid et al., 2013). In our studies Nox4 mRNA was not significantly elevated in the obese ZSF1 animals implying Nox4 is not a major contributor to renal dysfunction in this model (Eid et al., 2013). Nevertheless, Nox4 mRNA was modestly decreased in the 30 mg/kg PF-249 dose group ($P<0.05$) (Figure 6c).

In diabetic kidney models the transcriptional regulator PGC1 α , a well-known target of AMPK, has been linked to the modulation of mitochondrial function and the accompanying changes in the oxidative potential and ROS generation (Dugan et al., 2013). While PGC1 α mRNA was similar in the obese and lean ZSF1 groups, an increase in the PGC1 α transcript was observed in the 30 mg/kg PF-249 treated animals (Figure 6d). The modest changes in whole tissue mRNA levels of the markers of kidney disease in this study may be ascribed to the multiple cell types comprising the nephron. Consequently, these mRNA-based transcriptomics studies were inconclusive in defining a specific mechanism downstream of AMPK activation responsible for the observed improvements in kidney function.

Discussion

Disease modifying therapies are needed to stem the tide of renal disease in the burgeoning population of individuals with the metabolic syndrome. To this end, AMPK activation has shown some promise in this therapeutic area based on the use of imperfect indirect activators that are unlikely to be effective clinically. Here we describe the identification of PF-06409577 and PF-249, and demonstrate the ability of each to selectively activate AMPK heterotrimers that contain the $\beta 1$ subunit and modify the rate of disease progression in the ZSF1 rat model of DN.

Both PF-06409577 and PF-249 improve kidney function, with robust reductions in proteinuria that are stable over a treatment duration of more than 2 months. Interestingly, the profile of proteinuria improvement appears distinct as compared with the ACEi ramipril, which lowers UACR more rapidly but fails to alter the disease progression slope. In contrast, AMPK activation by either compound resulted in an effect that was not evident at two weeks of treatment but appeared to alter the rate of increased proteinuria. However, the relationship of the observed effects in the animal model to true delay in disease progression in man is unclear. Nevertheless, the potential for beneficial effects of AMPK activation in multiple relevant cell types in the kidney suggests advantages of this novel approach for the treatment of DN compared to the current standard of care. The reduced mTOR signaling in the glomeruli following PF-06409577 treatment suggests that suppression of this hypertrophic pathway by AMPK activation could be one source of AMPK-mediated benefit in this DN model. We observed improvement in urinary markers of specific disease processes, including the oxidative stress marker TBARs, fibrotic marker TIMP1, and the general kidney injury marker KIM1, in addition to reduction of proteinuria. While treatment did not cause a large drop in systemic blood pressure, there were modest decreases observed at some time periods that could contribute to the observed improvements in disease. Nevertheless, because of the complexity of renal pathology, which includes inflammation, fibrosis, tubular damage, systemic blood

pressure dynamic, and glomerular sclerosis, it is unlikely that a single protective mechanism underlies the observed pharmacological effects.

The selective small molecule activators of AMPK β 1-containing heterotrimers described here dramatically improve renal function in a rodent model of diabetic nephropathy. These results suggest that activators of AMPK warrant further testing as a treatment for human diabetic nephropathy, and potentially other kidney diseases that remain inadequately treated by existing medicines.

Author Contributions

C.S., R.M., K.C., J.W., M.B., P.D., and T.R. participated in research design. C.S., R.M., E.C., A.R., J.W., A.K., D.T., A.J., B.M., M.A., H.G., M.M., K.C., E.B., J.K., T.C., G.B., and A.O. conducted experiments.. K.C, A.S., N.G., M.C., F.R, and D.E. contributed new reagents or analytical tools. C.S., R.M., K.C., E.C., A.R., J.W., M.C., R.K., A.K., D.E., M.M., M.B., and T.R. wrote or contributed to the writing of the manuscript.

References

- Bilan VP, Salah EM, Bastacky S, Jones HB, Mayers RM, Zinker B, Poucher SM and Tofovic SP (2011) Diabetic nephropathy and long-term treatment effects of rosiglitazone and enalapril in obese ZSF1 rats. *J Endocrinol* **210**:293-308.
- Blanc E, Roversi P, Vornrhein C, Flensburg C, Lea SM and Bricogne G (2004) Refinement of severely incomplete structures with maximum likelihood in BUSTER-TNT. *Acta crystallographica Section D, Biological crystallography* **60**:2210-2221.
- Boustany-Kari CM, Harrison PC, Chen H, Lincoln KA, Qian HS, Clifford H, Wang H, Zhang X, Gueneva-Boucheva K, Bosanac T, Wong D, Fryer RM, Richman JG, Sarko C and Pullen SS (2016) A Soluble Guanylate Cyclase Activator Inhibits the Progression of Diabetic Nephropathy in the ZSF1 Rat. *J Pharmacol Exp Ther* **356**:712-719.
- Calabrese MF, Rajamohan F, Harris MS, Caspers NL, Magyar R, Withka JM, Wang H, Borzilleri KA, Sahasrabudhe PV, Hoth LR, Geoghegan KF, Han S, Brown J, Subashi TA, Reyes AR, Frisbie RK, Ward J, Miller RA, Landro JA, Londregan AT, Carpino PA, Cabral S, Smith AC, Conn EL, Cameron KO, Qiu X and Kurumbail RG (2014) Structural basis for AMPK activation: natural and synthetic ligands regulate kinase activity from opposite poles by different molecular mechanisms. *Structure* **22**:1161-1172.
- Cameron KO, Kung DW, Kalgutkar AS, Kurumbail RG, Miller R, Salatto CT, Ward J, Withka JM, Bhattacharya SK, Boehm M, Borzilleri KA, Brown JA, Calabrese M, Caspers NL, Cokorinos E, Conn EL, Dowling MS, Edmonds DJ, Eng H, Fernando DP, Frisbie R, Hepworth D, Landro J, Mao Y, Rajamohan F, Reyes AR, Rose CR, Ryder T, Shavnya A, Smith AC, Tu M, Wolford AC and Xiao J (2016) Discovery and Preclinical Characterization of 6-Chloro-5-[4-(1-hydroxycyclobutyl)phenyl]-1H-indole-3-carboxylic Acid (PF-06409577), a Direct Activator of Adenosine Monophosphate-activated Protein Kinase (AMPK), for the Potential Treatment of Diabetic Nephropathy. *J Med Chem* **59**:8068-8081.
- Dugan LL, You YH, Ali SS, Diamond-Stanic M, Miyamoto S, DeClevés AE, Andreyev A, Quach T, Ly S, Shekhtman G, Nguyen W, Chepetan A, Le TP, Wang L, Xu M, Paik KP, Fogo A, Viollet B, Murphy A, Brosius F, Naviaux RK and Sharma K (2013) AMPK dysregulation promotes diabetes-related reduction of superoxide and mitochondrial function. *J Clin Invest* **123**:4888-4899.
- Eid AA, Ford BM, Bhandary B, de Cassia Cavaglieri R, Block K, Barnes JL, Gorin Y, Choudhury GG and Abboud HE (2013) Mammalian target of rapamycin regulates Nox4-mediated podocyte depletion in diabetic renal injury. *Diabetes* **62**:2935-2947.
- Emsley P and Cowtan K (2004) Coot: model-building tools for molecular graphics. *Acta crystallographica Section D, Biological crystallography* **60**:2126-2132.
- Gallagher H and Suckling RJ (2016) Diabetic nephropathy - where are we on the journey from pathophysiology to treatment? *Diabetes, obesity & metabolism*.
- Godel M, Hartleben B, Herbach N, Liu S, Zschiedrich S, Lu S, Debreczeni-Mor A, Lindenmeyer MT, Rastaldi MP, Hartleben G, Wiech T, Fornoni A, Nelson RG, Kretzler M, Wanke R, Pavenstadt H, Kerjaschki D, Cohen CD, Hall MN, Ruegg MA, Inoki K, Walz G and Huber TB (2011) Role of mTOR in podocyte function and diabetic nephropathy in humans and mice. *J Clin Invest* **121**:2197-2209.
- Hallows KR, Mount PF, Pastor-Soler NM and Power DA (2010) Role of the energy sensor AMP-activated protein kinase in renal physiology and disease. *Am J Physiol Renal Physiol* **298**:F1067-1077.
- Inoki K and Huber TB (2012) Mammalian target of rapamycin signaling in the podocyte. *Curr Opin Nephrol Hypertens* **21**:251-257.

- Inoki K, Mori H, Wang J, Suzuki T, Hong S, Yoshida S, Blattner SM, Ikenoue T, Ruegg MA, Hall MN, Kwiatkowski DJ, Rastaldi MP, Huber TB, Kretzler M, Holzman LB, Wiggins RC and Guan KL (2011) mTORC1 activation in podocytes is a critical step in the development of diabetic nephropathy in mice. *J Clin Invest* **121**:2181-2196.
- Kim D, Lee JE, Jung YJ, Lee AS, Lee S, Park SK, Kim SH, Park BH, Kim W and Kang KP (2013) Metformin decreases high-fat diet-induced renal injury by regulating the expression of adipokines and the renal AMP-activated protein kinase/acetyl-CoA carboxylase pathway in mice. *Int J Mol Med* **32**:1293-1302.
- Kottgen A, Pattaro C, Boger CA, Fuchsberger C, Olden M, Glazer NL, Parsa A, Gao X, Yang Q, Smith AV, O'Connell JR, Li M, Schmidt H, Tanaka T, Isaacs A, Ketkar S, Hwang SJ, Johnson AD, Dehghan A, Teumer A, Pare G, Atkinson EJ, Zeller T, Lohman K, Cornelis MC, Probst-Hensch NM, Kronenberg F, Tonjes A, Hayward C, Aspelund T, Eiriksdottir G, Launer LJ, Harris TB, Rumpersaud E, Mitchell BD, Arking DE, Boerwinkle E, Struchalin M, Cavalieri M, Singleton A, Giallauria F, Metter J, de Boer IH, Haritunians T, Lumley T, Siscovick D, Psaty BM, Zillikens MC, Oostra BA, Feitosa M, Province M, de Andrade M, Turner ST, Schillert A, Ziegler A, Wild PS, Schnabel RB, Wilde S, Munzel TF, Leak TS, Illig T, Klopp N, Meisinger C, Wichmann HE, Koenig W, Zgaga L, Zemunik T, Kolcic I, Minelli C, Hu FB, Johansson A, Igl W, Zaboli G, Wild SH, Wright AF, Campbell H, Ellinghaus D, Schreiber S, Aulchenko YS, Felix JF, Rivadeneira F, Uitterlinden AG, Hofman A, Imboden M, Nitsch D, Brandstatter A, Kollerits B, Kedenko L, Magi R, Stumvoll M, Kovacs P, Boban M, Campbell S, Endlich K, Volzke H, Kroemer HK, Nauck M, Volker U, Polasek O, Vitart V, et al. (2010) New loci associated with kidney function and chronic kidney disease. *Nat Genet* **42**:376-384.
- Lee MJ, Feliers D, Mariappan MM, Sataranatarajan K, Mahimainathan L, Musi N, Foretz M, Viollet B, Weinberg JM, Choudhury GG and Kasinath BS (2007) A role for AMP-activated protein kinase in diabetes-induced renal hypertrophy. *Am J Physiol Renal Physiol* **292**:F617-627.
- Mihaylova MM and Shaw RJ (2011) The AMPK signalling pathway coordinates cell growth, autophagy and metabolism. *Nat Cell Biol* **13**:1016-1023.
- Otinowski Z and Minor W (1997) Processing of X-ray Diffraction Data Collected in Oscillation Mode. *Methods Enzymol* **276**:307-326.
- Rajamohan F, Reyes AR, Ruangsiriluk W, Hoth LR, Han S, Caspers N, Tu M, Ward J and Kurumbail RG (2015) Expression and functional characterization of human lysosomal acid lipase gene (LIPA) mutation responsible for cholesteryl ester storage disease (CESD) phenotype. *Protein Expr Purif* **110**:22-29.
- Sharma K, Ramachandrarao S, Qiu G, Usui HK, Zhu Y, Dunn SR, Ouedraogo R, Hough K, McCue P, Chan L, Falkner B and Goldstein BJ (2008) Adiponectin regulates albuminuria and podocyte function in mice. *J Clin Invest* **118**:1645-1656.
- Steinberg GR and Kemp BE (2009) AMPK in Health and Disease. *Physiol Rev* **89**:1025-1078.
- Vallon V and Komers R (2011) Pathophysiology of the diabetic kidney. *Comprehensive Physiology* **1**:1175-1232.
- Yuan F, Liu YH, Liu FY, Peng YM and Tian JW (2014) Intraperitoneal administration of the globular adiponectin gene ameliorates diabetic nephropathy in Wistar rats. *Mol Med Rep* **9**:2293-2300.
- Zoja C, Cattaneo S, Fiordaliso F, Lionetti V, Zambelli V, Salio M, Corna D, Pagani C, Rottoli D, Bisighini C, Remuzzi G and Benigni A (2011) Distinct cardiac and renal effects of ETA receptor antagonist and ACE inhibitor in experimental type 2 diabetes. *Am J Physiol Renal Physiol* **301**:F1114-1123.

Figure Legends

Figure 1

A. *In vitro* AMPK activity for selected AMPK heterotrimers ($\alpha\beta\gamma$) activated with PF-06409577. **B.** *In vitro* AMPK activity for selected AMPK heterotrimers ($\alpha\beta\gamma$) activated with PF-249. **C.** Ribbon representation of crystal structure of AMPK $\alpha 1\beta 1\gamma 1$ bound to PF-249. **D.** A close-up view of the ligand-protein interface. **E.** AMPK β subunit levels in kidney tissue was measured by quantitative ELISA and plotted as percent AMPK heterotrimer containing the $\beta 1$ subunit. $\beta 1$ subunit protein content (based on summation of both $\beta 1$ and $\beta 2$ subunits) is also shown for each species in pmol/g tissue.

Figure 2

A. Western blot for AMPK $\beta 1$, $\beta 2$, and pan- α in 293FT cells transfected with scrambled siRNA or siRNA targeting AMPK $\beta 1$. **B.** ELISA quantification of ACC phosphorylation status in 293FT treated with siRNA and PF-06409577. **C.** ELISA quantification of ACC phosphorylation status in 293FT treated with siRNA and PF-06409577. ** indicates $p < 0.01$.

Figure 3

A. Cumulative urinary albumin excretion over a 24 hour period at multiple time points during a dosing study in obese ZSF1 rats treated with vehicle or PF-06409577; 10 or 11 animals per group. **B.** Kidney AMPK phosphorylation status in terminal samples after 8 weeks of dosing, 1 hour after the last dose. Values are normalized such that the obese vehicle group is equal to 100. Significance is indicated compared to the vehicle; 10-11 animals per group. **C-D.** Fasted blood glucose and insulin after 8 weeks of dosing. **E-F.** Mean blood pressure in telemeterized ZSF1 rats treated with vehicle, 10, 30, or 100 mg/kg of PF-06409577. Data are presented as

the fold change from the vehicle group during defined periods throughout day 6 and 14. *

denotes $p < 0.05$, ** $p < 0.01$, *** $p < 0.001$.

Figure 4

A. Cumulative albumin excretion over a 24 hour period at multiple time points during a dosing study in ZSF1 rats treated with vehicle, PF-249, PF-06409577, or Ramipril (1 mg/kg/day in drinking water); 12 animals per group. **B.** Kidney AMPK phosphorylation status in terminal samples after 8 weeks of dosing, 1 hour after the last dose. Values are normalized such that the obese vehicle group equals 100. Significance is indicated compared to the vehicle; 10-11 animals per group. * denotes $p < 0.05$, ** $p < 0.01$, *** $p < 0.001$.

Figure 5

A-C. Representative histology images of phospho-S6 (p-S6) reactivity in kidneys collected after 8 weeks of dosing vehicle or PF-06409577 to ZSF1 rats; 12 animals per group. Glomeruli are indicated by the arrows and stain area was quantified. **D.** Quantitative measure of p-S6 stain area in glomeruli of 5 lean ZSF1 treated with vehicle, 7 obese ZSF1 treated with vehicle, and 7 obese ZSF1 animals treated with PF-06409577. ** denotes $p < 0.01$

Figure 6

Quantitative PCR measurements of mRNA for **A.** *Col1a1*, **B.** *Col4a1*, **C.** *Nox4*, and **D.** *Ppargc1a* in kidney samples from animals treated with 3, 10, and 30 mg/kg PF-249, 100 mg/kg PF-06409577 (PF-577), or ramipril for 8 weeks; 8-10 animals per group. Significance compared to the obese vehicle group. ** denotes $p < 0.01$

JPET #237925

Table

Table 1

Measures of urinary biomarkers of kidney function after 8 weeks dosing of vehicle, PF-249, PF-06409577, or ramipril.

	Lean Vehicle	Obese Vehicle	3 mg/kg PF-249	10 mg/kg PF-249	30mg/kg PF-249	100 mg/kg PF- 06409577	Ramipril
UACR (mg/mg)	0.04 (0.03) ****	20.32 (3.4)	15.9 (4.8) *	13.34 (3.06) ***	5.34 (3.23) ****	5.23 (4.54) ****	9.00 (5.87) ****
UPCR (mg/mg)	2.39 (0.14) ****	25.56 (1.53)	20.32 (1.75)*	17.29 (1.09) ***	7.56 (1.06) ****	7.47 (1.48) ****	12.10 (1.93) ****
TBARs/crea (nmol/mg)	0.09 (0.01) ****	0.17 (0.04)	0.16 (0.03)	0.14 (0.04)	0.12 (0.03) **	0.12 (0.04) **	0.12 (0.05) **
TIMP1/crea (ng/mg)	47.68 (15.84) ****	127.79 (30.51)	114.91 (22.17)	103.5 (16.22)	68.33 (16.52)****	65.70 (25.69) ****	97.15 (40.76) *
KIM1/crea (pg/mg)	3.30 (0.12) ****	12.36 (4.08)	11.78 (3.63)	10.74 (5.44)	6.72 (2.51) **	6.96 (3.83) **	7.05 (1.85) **

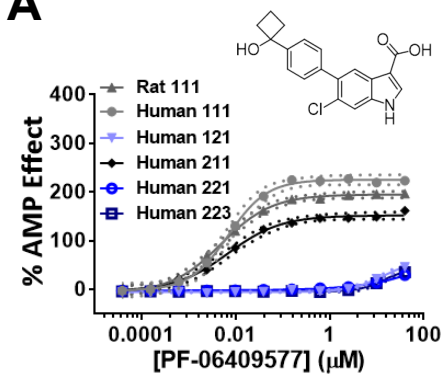
Downloaded from jpet.aspetjournals.org at ASPET Journals on March 20, 2024

JPET #237925

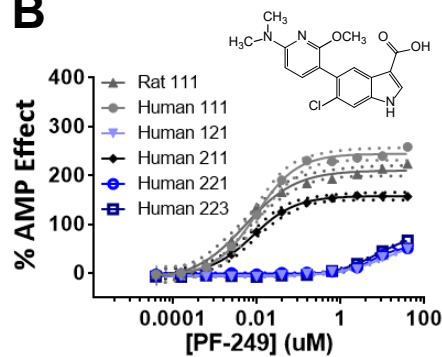
Samples are measured from urine samples collected over a 24 hour period; 11-12 animals per group. * denotes $p < 0.05$, ** $p < 0.01$, *** $p < 0.001$, **** $p < 0.0001$. UACR: urinary albumin creatinine ratio; UPCR: urinary protein creatinine ratio; TBARs; thiobarbituric acid reactive substances; TIMP1: tissue metalloprotease inhibitor-1; KIM-1: kidney injury marker-1.

Figure 1

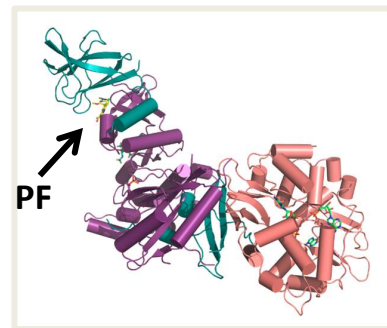
A



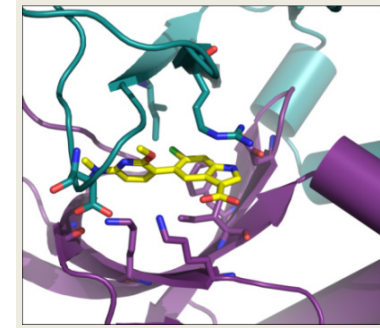
B



C



D



E

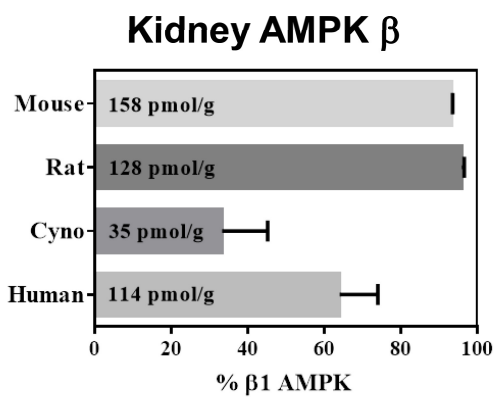
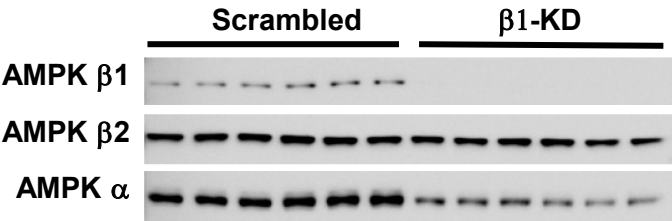
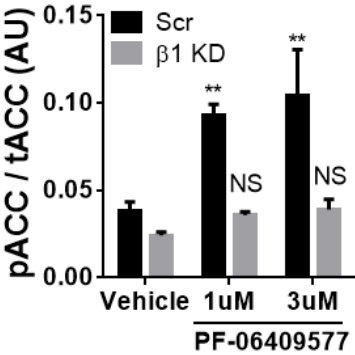


Figure 2

A



B



C

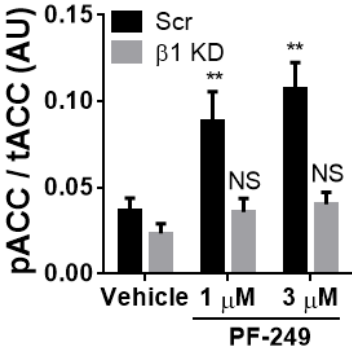
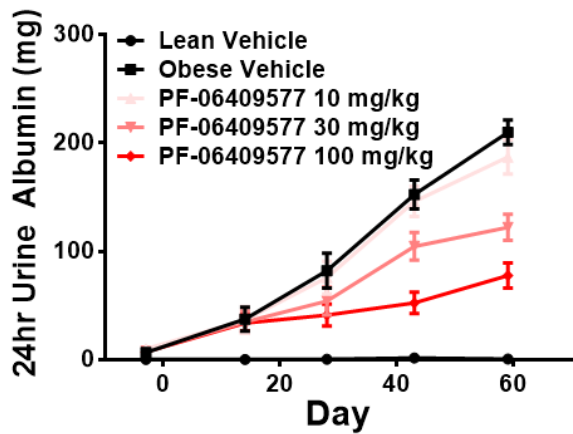
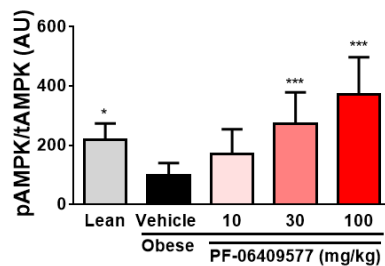


Figure 3

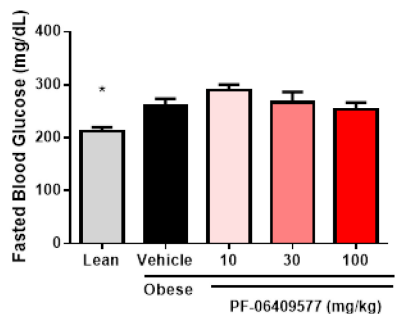
A



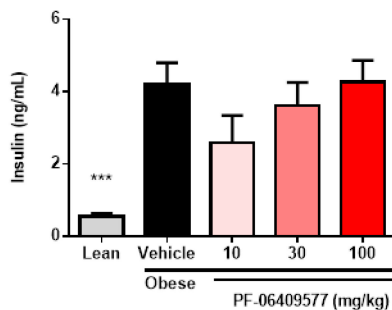
B



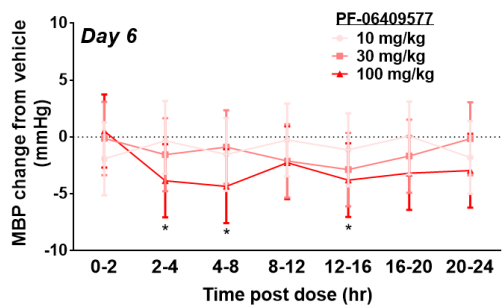
C



D



E



F

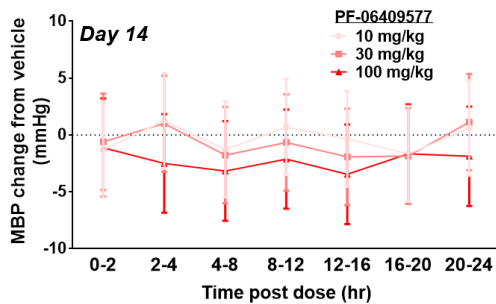


Figure 4

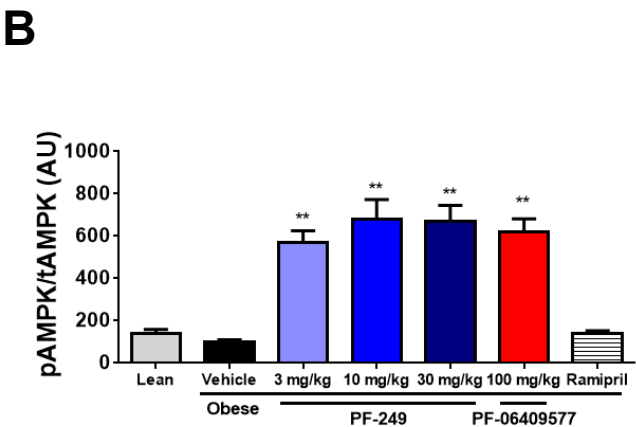
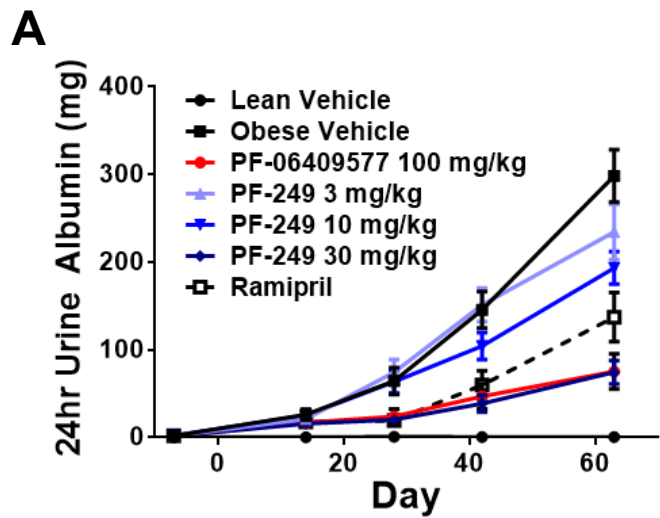


Figure 5

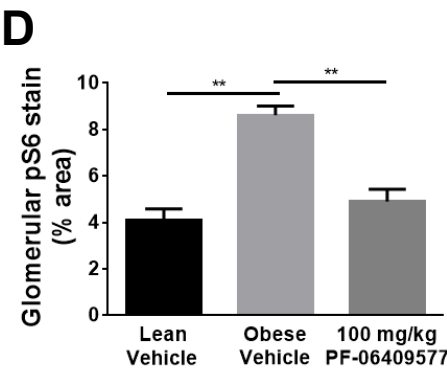
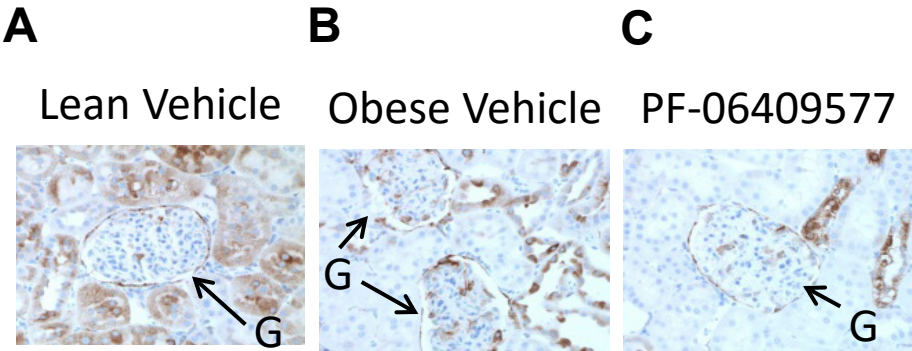
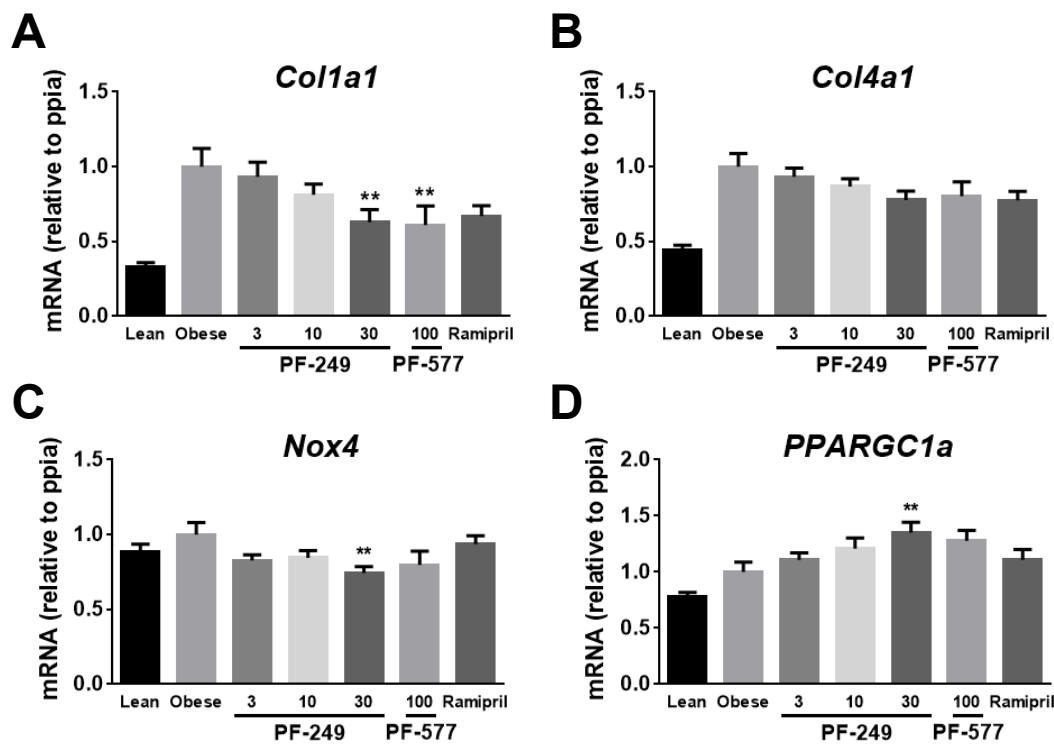


Figure 6



Supplemental Data

Selective Activation of AMPK β 1-containing Isoforms Improves Kidney Function in a Rat Model of Diabetic Nephropathy

Christopher T Salatto, Russell A Miller, Kimberly O Cameron, Emily Cokorinos, Allan Reyes, Jessica Ward, Matt Calabrese, Ravi Kurumbail, Francis Rajamohan, Amit S Kalgutkar, David A. Tess, Andre Shavnya, Nathan E Genung, David J Edmonds, Aditi Jatkar, Benjamin S Maciejewski, Marina Amaro, Harmeet Gandhok, Mara Monetti, Katherine Cialdea, Eliza Bollinger, John M Kreeger, Timothy M Coskran, Alan C Opsahl, Germaine G Boucher, Morris J Birnbaum, Paul DaSilva-Jardine and Tim Rolph

CVMET Research Unit, Pfizer World Wide Research and Development, Cambridge MA, 02139 (CS, RM, EC, AR, JW, AJ, BM, MA, HG, MM, KC, EB, MB, PD, TR)

Worldwide Medicinal Chemistry, Pfizer World Wide Research and Development, Cambridge MA, 02139 (KC, DE)

Worldwide Medicinal Chemistry, Pfizer World Wide Research and Development, Groton CT, 06340 (MC, RK, FR, AS, NG)

Pharmacokinetics, Dynamics, & Metabolism, Pfizer World Wide Research and Development, Cambridge MA, 02139 (AK, DT)

Drug Safety Research and Development, Pfizer World Wide Research and Development, Groton CT, 06340 (JK, TC, AO, GB)

Co-corresponding authors (CS, RM)

Supplemental Methods**Synthesis and characterization of PF-06409577**

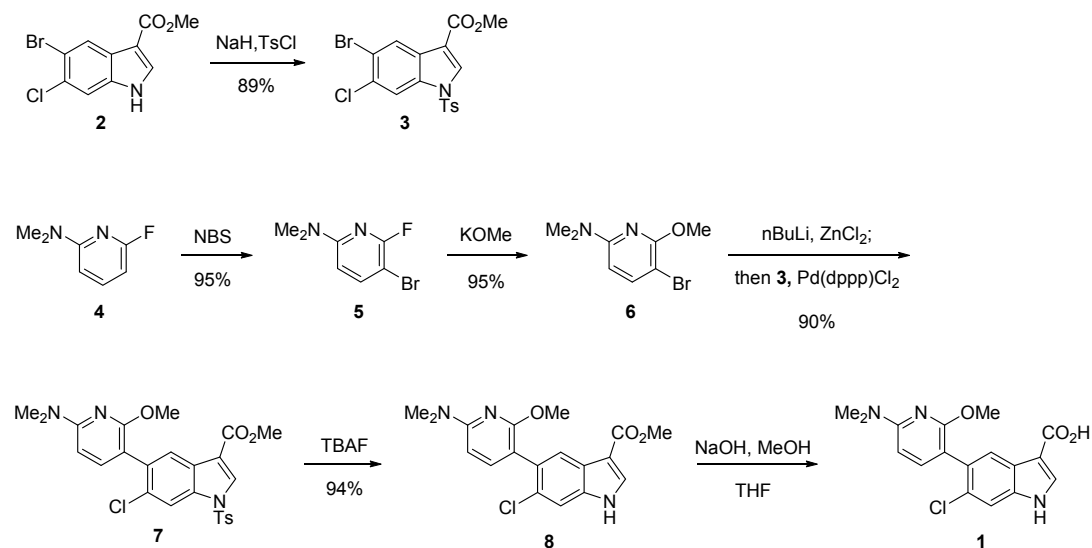
Reported in (1). PF-06409577 is commercially available from Sigma Aldrich (#PZ0319)

Synthesis and characterization of 6-chloro-5-(6-(dimethylamino)-2-methoxypyridin-3-yl)-1H-indole-3-carboxylic acid PF-249 (1)

General Experimental Methods. All reagents and solvents were obtained from commercial suppliers and used without further purification, unless otherwise noted. Silica gel chromatography was performed using medium pressure ISCO systems employing columns pre-packaged by commercial vendors. ¹H and ¹³C NMR characterization data were collected at 300 K on either a spectrometer operating at 600 and 151 MHz (respectively) or a spectrometer operating at 400 and 100 MHz (respectively). Chemical shifts reported in parts per million relative to CHCl₃ (¹H NMR; 7.26 ppm, ¹³C NMR; 77.23 ppm). ¹H NMR data are reported as follows: chemical shift (multiplicity, coupling constant (Hz), number of hydrogens).

II. Procedures to Synthesize PF-249 (1, Scheme 1)

Scheme 1



Methyl 5-bromo-6-chloro-1-tosyl-1H-indole-3-carboxylate (3): To a solution of 5-bromo-6-chloro-1*H*-indole-3-carboxylic acid methyl ester (80.0 g, 277 mmol) in *N,N*-dimethylformamide (600 mL) at 0 °C was added sodium hydride (60% dispersion in oil, 16.6 g, 416 mmol) portion-wise over 20 minutes. The reaction was stirred at 0 °C for 60 minutes followed by the addition of 4-methylbenzenesulphonyl chloride (63.4 g, 333 mmol), which was added portion-wise to the stirring solution. The reaction was stirred for 2 hours at 0 °C, the ice bath was removed and the reaction was warmed to room temperature and stirred overnight. The reaction was poured into water (1200 mL) and stirred for 12 hours. The suspension was filtered and the filter cake was washed with a further portion of water (700 mL) followed by heptane (2 x 300 mL) to provide 160 g of crude product.. The material was placed in a 3 L round bottom flask and placed under vacuum on a rotary evaporator with a 40°C bath overnight to remove residual water. This afforded 116 g of a pink solid which was suspended in acetone (600 mL) and heated to reflux for 1 hour, removed from the heat, cooled to room temperature, and stirred for 1 hour. The suspension was filtered and the filter cake was washed with acetone until the filtrate was colorless (~500 mL). The filter cake was dried to afford desired product (108.7 g, 89% yield). ¹H NMR (CDCl₃, 400 MHz) δ 8.39 (s, 1H) 8.24 (s, 1H) 8.11 (s, 1H) 7.82 (d, *J* = 8.6 Hz, 2H) 7.32 (d, *J* = 8.2 Hz, 2H) 3.93 (s, 3H) 2.40 (s, 3H). HRMS (ESI) *m/z* calculated for C₁₇H₁₃ClNO₄S (M+H)⁺ 443.9488, observed: 443.9482.

5-Bromo-6-fluoro-N,N-dimethylpyridin-2-amine (5): To a solution of 6-fluoro-N,N-dimethylpyridin-2-amine (12.4 g, 88.4 mmol) in acetonitrile (400 mL) at 0 °C was added a solution of *N*-bromosuccinimide (7.87 g, 44.2 mmol) in acetonitrile (95 mL) dropwise over 15 min. The resulting solution was stirred at 0 °C for 1 hour. Another portion of *N*-bromosuccinimide (7.87 g, 44.2 mmol) in acetonitrile (95 mL) was subsequently added at 0 °C dropwise over 15 min. The solution was slowly warmed to room temperature and stirred overnight. The solution was concentrated *in vacuo* and diluted with dichloromethane (500 mL).

This solution was washed with water (300 mL) and the aqueous layer was washed with dichloromethane (3 x 200 mL). The combined organic layers were dried (MgSO_4), filtered, and concentrated *in vacuo*. The material was passed through a silica pad, eluting with 0-10% ethyl acetate in heptanes. The organic solutions were concentrated *in vacuo* to afford the desired material (18.4 g, 95% yield) which solidified upon standing.

^1H NMR (CDCl_3 , 400 MHz) δ 7.48 - 7.67 (m, 1H) 6.21 (dd, J = 8.6, 1.6 Hz, 1H) 3.05 (s, 6H).

GCMS (EI) m/z calculated for $\text{C}_7\text{H}_8\text{BrFN}_2$ (M)⁺ 218.0, observed: 218.0.

5-Bromo-6-methoxy-N,N-dimethylpyridin-2-amine (6): To a solution of potassium methoxide (25% in methanol, 74.2 mL, 251 mmol) was added 5-bromo-6-fluoro-N,N-dimethylpyridin-2-amine (18.36 g, 83.8 mmol). The reaction was heated at reflux for 3 h and was cooled to room temperature. The contents were poured into a solution of saturated ammonium chloride (500 mL) and the aqueous solution was extracted with ethyl acetate (3 x 300 mL). The combined organic layers were washed with brine (250 mL), dried over MgSO_4 , filtered, and concentrated *in vacuo* to afford the desired product as an oil that solidified upon standing to give an off-white/yellow solid (18.3 g, 95% yield).

^1H NMR (CDCl_3 , 400 MHz) δ 7.49 (d, J = 8.6 Hz, 1H) 5.95 (d, J = 8.6 Hz, 1H) 3.96 (s, 3H) 3.05 (s, 6H). GCMS (EI) m/z calculated for $\text{C}_8\text{H}_{11}\text{BrN}_2\text{O}$ (M)⁺ 230.0, observed: 230.0.

Methyl 6-chloro-5-(6-(dimethylamino)-2-methoxypyridin-3-yl)-1-tosyl-1H-indole-3-

carboxylate (7): To a solution of 5-bromo-6-methoxy-N,N-dimethylpyridin-2-amine (78.8 g, 341 mmol) in THF (400 mL) at -70 °C was added a solution of *n*-butyllithium (2.5 M in hexanes, 127 mL, 317 mmol) dropwise, keeping the internal temperature below -60 °C. The purple solution was stirred between -65 °C and -70 °C for 20 min. A solution of ZnCl_2 in 2-methyltetrahydrofuran (1.9 M, 167 mL, 320 mmol) was added dropwise to the aryl lithium solution, keeping the internal temperature below -60 °C. The resulting mixture was stirred between -65 °C and -70 °C for 20 min, was warmed to room temperature, and stirred for 2 h.

The clear, pale yellow aryl zinc solution was cannulated into a flask containing methyl 5-bromo-6-chloro-1-tosyl-1H-indole-3-carboxylate (107.8 g, 244 mmol) and dichloro[bis(2-(diphenylphosphino)phenyl)ether]palladium(II) (8.72 g, 12.2 mmol) in THF (200 mL). The resulting mixture was stirred at room temperature for 2.5 h and was quenched with saturated aqueous NH_4Cl (800 mL). The aqueous solution was extracted with ethyl acetate (1500 mL and 750 mL) and the combined organic layers were washed with brine (1000 mL), dried over MgSO_4 , filtered, and concentrated *in vacuo*. The residue was triturated with methanol (~600 mL) and was stirred overnight. The suspension was filtered to give a tan solid. This solid was dissolved in hot acetone (2 L) which was partially concentrated to ~500 mL and slowly cooled and stirred overnight. The resulting solid was filtered to yield one crop of desired product (109.1 g). The filtrate was concentrated to a dark solid which was slurried in acetone and filtered. The resulting solid was dissolved in hot acetone and was cooled to yield a second crop (3.3 g) of desired product as an off-white solid. (90% total yield).

^1H NMR ($\text{DMSO}-d_6$, 400 MHz) δ 8.51 (s, 1H), 8.11 (d, $J = 8.6$ Hz, 2H), 8.00 (s, 1H), 7.88 (s, 1H), 7.49 (d, $J = 8.2$ Hz, 2H), 7.31 (d, $J = 8.2$ Hz, 1H), 6.22 (d, $J = 8.2$ Hz, 1H), 3.84 (s, 3H), 3.74 (s, 3H), 3.06 (s, 6H), 2.37 (s, 3H). HRMS (ESI) m/z calculated for $\text{C}_{25}\text{H}_{24}\text{ClN}_3\text{O}_5\text{S}$ ($\text{M}+\text{H}$) $^+$ 514.1198, observed: 514.1196.

Methyl 6-chloro-5-(6-(dimethylamino)-2-methoxypyridin-3-yl)-1H-indole-3-carboxylate (8):

To a solution of methyl 6-chloro-5-(6-(dimethylamino)-2-methoxypyridin-3-yl)-1-tosyl-1H-indole-3-carboxylate (109 g, 212 mmol) in THF (1000 mL) at room temperature was added tetrabutylammonium fluoride (1.0 M in THF, 400 mL, 400 mmol). The reaction was heated at reflux for 3 h before cooling to room temperature and diluting with ethyl acetate (2000 mL). The organic solution was washed sequentially with saturated aqueous NaHCO_3 (2 x 750 mL), saturated aqueous NH_4Cl (2 x 750 mL), water (750 mL), and brine (750 mL). The organic solution was dried over MgSO_4 , filtered, and concentrated *in vacuo*. The residue was triturated

with methanol (~500 mL) and filtered. The solids were washed with methanol (300 mL) and suction dried overnight to afford desired product (71.8 g, 94%) as a white solid.

^1H NMR (DMSO- d_6 , 400 MHz) δ 11.99 (s, 1H) 8.13 (s, 1H) 7.82 (s, 1H) 7.57 (s, 1H) 7.32 (d, J = 8.2 Hz, 1H) 6.22 (d, J = 8.2 Hz, 1H) 3.78 (s, 3H) 3.76 (s, 3H) 3.07 (s, 6H). HRMS (ESI) m/z calculated for $\text{C}_{18}\text{H}_{18}\text{ClN}_3\text{O}_3$ ($\text{M}+\text{H}$) $^+$ 360.1109, observed: 360.1110.

6-Chloro-5-(6-(dimethylamino)-2-methoxypyridin-3-yl)-1H-indole-3-carboxylic acid (1): To a solution of methyl 6-chloro-5-(6-(dimethylamino)-2-methoxypyridin-3-yl)-1H-indole-3-carboxylate (45.0 g, 130 mmol) in 1:1 tetrahydrofuran : methanol (1250 mL) at 50 °C was added 2 N NaOH (1250 mL). After stirring for 60h, the reaction was cooled to < 5 °C and, with stirring, 6 N HCl (417 mL) was added dropwise to achieve pH 6-7. The solution was divided in half and each was diluted with ethyl acetate (1.5 L) and the layers separated. The aqueous layers were back extracted with ethyl acetate (2 x 600 mL). The organic solutions were combined and washed with saturated aqueous NH_4Cl (1 L) followed by brine (1 L), and dried over MgSO_4 , filtered and concentrated *in vacuo* to give crude product. Several batches of crude product were combined (117 g) and acetone (3.5 L) was added. This was heated at reflux to dissolve all solids, concentrated to ~1.5 L, and slowly cooled. These resulting precipitate was suspended in heptanes (~500 mL) and the mixture was stirred at 80 °C for 48 h. Solids were collected by filtration and suction dried for 15 h to afford the desired product (80.0 g) as a solid.

^1H NMR (DMSO- d_6 , 400 MHz) δ 12.03 (br. s, 1H) 11.86 (br. s, 1H) 8.04 (d, J = 2.7 Hz, 1H) 7.83 (s, 1H) 7.55 (s, 1H) 7.32 (d, J = 8.2 Hz, 1H) 6.21 (d, J = 8.2 Hz, 1H) 3.76 (s, 3H) 3.07 (s, 6H). HRMS (ESI) m/z calculated for $\text{C}_{17}\text{H}_{16}\text{ClN}_3\text{O}_3$ ($\text{M}+\text{H}$) $^+$ 346.0953, observed: 346.0953.

Reagents

siRNA targeting human *PRKAB1* was purchased from Life Technologies, duplex s11060.

Silencer Select negative control #1 (#4390843) was used as scrambled control. AMPK pan-

alpha #5831, AMPK β 1 #4178, AMPK β 2 #4148, and Acetyl-CoA Carboxylase #3676 antibodies were purchased from Cell Signaling Technologies (Danvers, MA). AMPK alpha 1 + AMPK alpha 2 antibody #ab80039 was purchased from Abcam (Cambridge, MA).

Materials for activation and protection assays – Recombinant AMPK complexes were cloned, expressed in E coli and purified as described previously (2). The Europium-labeled anti phospho SAMS (S79) antibody was generated by custom labeling a Millipore (Billerica, MA) mouse monoclonal pACC antibody with Europium Lantha screen Amine reactive chelate (Invitrogen, MA). Human PP2Ac alpha1 (Uniprot P67775-1) was expressed and purified as described previously with some changes (3). N-term His10x-tagged PP2a was expressed in Sf9 cells and purified using HisTrapTM FF (GE Healthcare) and Q Fast Flow (GE Healthcare) chromatographies.

Chemical Synthesis of Cy5 conjugate of SAMS peptide.

The Acetyl-CoA carboxylase (S79)SAMS peptide (CHMRSAMSGHLHLVKRR) was synthesized by American Peptide and labeled with the Cy5 fluorophore in-house. To a solution of 14.0 mg (5 μ mol) SAMS peptide in 0.5 mL 50% acetonitrile/water was added 3 mg (3.85 μ mol) Cy5 mono maleimide, and 0.3 mL 1 M sodium acetate pH 5. After 15 minutes, the reaction was purified directly by preparative HPLC. Preparative high-performance liquid chromatography (HPLC) was performed using a Waters SunFire C18 OBD Prep Column, 130Å, 5 μ m, 19 mm X 100 mm (Waters, part number 186002567), eluting with a linear slope gradient at 17 mL/min flow rate. Solvent gradient: Acetonitrile/water/trifluoroacetic acid (TFA) (2:98:0.1) to (32:68:0.1) in 30 min. Collected fractions were analyzed by analytical LCMS, and those judged as having adequate purity were pooled and evaporated. Concentration was estimated by UV absorbance at 649 nm (ϵ = 250,000 L/mol cm). ESMS: calculated m/z for desired product (M/5H⁺) = 532.66, found = 532.98.

Renal Histopathology

Methods for hematoxylin and eosin staining were as described in Materials and Methods. For EM, kidneys were fixed in buffered 4% formaldehyde/1% glutaraldehyde at 4°C. They were then rinsed in buffer, post fixed in buffered 1% OsO₄, dehydrated, embedded in epoxy resin and cured at 60°C.

Rat Pharmacokinetics

All experiments involving animals were conducted in our AAALAC-accredited facilities and were reviewed and approved by Pfizer Institutional Animal Care and Use Committee. Pharmacokinetic parameters were calculated from plasma concentration – time data and are reported as mean (\pm S.D. for $n=3$ and maximum values for $n=2$). Intravenous (i.v.) and oral (p.o.) pharmacokinetics were conducted in male Wistar-Han rats. Solution formulation for i.v. pharmacokinetics included 12% sulfobutylether- β -cyclodextrin (PF-06409577) or 10% DMSO/30% PEG400/60% water (PF-249). Oral pharmacokinetics were conducted using crystalline material in 0.5% methyl cellulose suspension and oral doses were administered to fasted animals.

Male jugular vein/carotid artery double cannulated Wistar-Han rats (253–315 g), obtained from Charles River Laboratories (Wilmington, MA), were fasted overnight and through the duration of the study (1.0 or 2.0 h), whereas access to water was provided *ad libitum*. PF-06409577 was administered intravenously (i.v.) ($n=3$ rats) in 12% sulfobutylether- β -cyclodextrin at a dose of 0.5 mg/kg, whereas PF-249 was administered i.v. ($n=2$) in 10% DMSO/30% PEG400/60% water at a dose of 1 mg/kg. The dosing volume for i.v. administration was 2.0 mL/kg and the i.v. bolus doses were administered via the carotid artery. Serial blood samples were collected before dosing and at 0.083, 0.25, 0.5, 1, 2, 4, 7, 24 h for both compounds with a 48 h sample also collected for PF-249 after dosing. PF-06409577 and PF-249 were also administered by p.o. gavage to rats (PF-06409577: 3, 10, and 30 mg/kg at 10 mL/kg in 0.5% methylcellulose, PF-

249: 3 mg/kg at 5 mL/kg in 0.5% methylcellulose). Blood samples were taken prior to p.o. administration then serial samples were collected at 0.25, 0.5, 1, 2, 4, 7, and 24 h after dosing. Blood samples were centrifuged to generate plasma. All plasma samples were kept frozen until analysis. Urine samples (0–7.0 and 7.0–24 h) were also collected after i.v. administration to rats. Aliquots of plasma or urine (30 μ L) were subjected to protein precipitation with acetonitrile containing indomethacin as internal standard. The supernatant was analyzed by liquid chromatography tandem mass spectrometry (LC-MS/MS) and concentrations of PF-06409577 and PF-249 in plasma and urine were determined by interpolation from a standard curve.

Determination of Pharmacokinetic Parameters

Pharmacokinetic parameters were determined using noncompartmental analysis (Watson v.7.4, Thermo Scientific, Waltham, MA). Maximum plasma concentrations (C_{\max}) of PF-06409577 and PF-249 in plasma after p.o. dosing in rats were determined directly from the experimental data, with T_{\max} defined as the time of first occurrence of C_{\max} . The area under the plasma concentration-time curve from $t = 0$ to 24 h (AUC_{0-24}) was estimated using the linear trapezoidal rule. Systemic plasma clearance (CL_p) was calculated as the intravenous dose divided by $AUC^{i.v.}$. The terminal rate constant (k_{el}) was calculated by a linear regression of the log-linear concentration-time curve, and the terminal elimination $t_{1/2}$ was calculated as 0.693 divided by k_{el} . Apparent steady state distribution volume (V_{dss}) was determined as the i.v. or p.o. dose divided by the product of AUC and k_{el} . The absolute bioavailability (F) of the p.o. doses was calculated by using the following equation: $F = AUC^{p.o.}/AUC^{i.v.} \times dose^{i.v.}/dose^{p.o.}$. Percentage of unchanged PF-06409577 and PF-249 excreted in urine over 24 h was calculated using the following equation: amount (in mg) of PF-06409577 or PF-249 in urine over the 24 h interval post dose/actual amount of PF-06409577 or PF-249 dose administered (mg) \times 100%. The renal clearance was derived as the ratio of amount (in mg) of PF-06409577 or PF-249 in urine over the 24 h interval post dose/ AUC_{0-24} .

LC-MS/MS Analysis for Quantitation of PF-06409577 and PF-249

Analyte concentrations were determined on AB Sciex QTrap5500, TurboSpray or AB Sciex API4000 LC-MS/MS triple quadrupole mass spectrometer (AB Sciex, Framingham, MA). Analytes were chromatographically separated using Shimadzu LC-20AD (Shimadzu Scientific Instruments, MD) pump. An CTC PAL autosampler was programmed to inject 20 μ L on: (a) XSELECT HSS T3 (2.5 μ m) 50 x 2 mm column using a mobile phase consisting of water with 0.1% formic acid (solvent A) and acetonitrile with 0.1% formic acid (solvent B) at a flow rate of 0.4 mL/min or (b) Eksigent 0.5 x 50 mm column using a mobile phase consisting of 0.1% formic acid in 10 mM ammonium formate (solvent A) and acetonitrile (solvent B) at a flow rate of 0.075 mL/min. Ionization was conducted in the negative ion mode at the ionspray interface temperature of 400 °C, using nitrogen for nebulizing and heating gas. PF-06409577, PF-249 and internal standards indomethacin or tolbutamide were detected using electrospray ionization in the multiple reaction monitoring mode monitoring for mass-to-charge (m/z) transition 340.20 \rightarrow 268.00, 346.09 \rightarrow 328.08, 356.50 \rightarrow 312.00, and 269.2 \rightarrow 170.0. Analyte standards were fit by least-squares regression of their areas to a weighted linear equation, from which the unknown concentrations were calculated. The linear dynamic range of the standard curve was 1–10000 ng/mL. All calibration standards were within \pm 20% of the nominal value.

PK/PD modeling of UACR-UPCR response

A pharmacokinetic/pharmacodynamic (PK/PD) model of ZSF-1 rat proteinuria (UPCR) and albuminuria (UACR) progression was developed to describe the observed concentration-time-effect relationships for PF-06409577 and PF-249 UPCR and UACR inhibition. First, naïve pool, 2-compartment pharmacokinetic (PK) models with first-order absorption (supplemental figure 4) were established to estimate the plasma concentration-time profiles of PF-06409577 and PF-249 in ZSF-1 rats. Next a naïve pool, phenomenological, disease progression model was constructed to describe the approximately time proportional progression of proteinuria and

albuminuria in ZSF-1 rats (Supplemental figure 4). With insufficient pharmacology data granularity to verify, PF-06409577 and PF-249 were assumed to directly inhibit the progression of proteinuria and albuminuria as prophylactics.

In the PF-06409577 dose response study in ZSF-1 rats, PF-06409577 was estimated to completely inhibit ($I_{max} = 100\%$) albuminuria and proteinuria progression with an unbound plasma concentration EC_{50} of 5.48 nM (Supplemental figures 5 and 6). In the PF-249 dose response study in ZSF-1 rats, PF-249 was estimated to completely inhibit ($I_{max} = 100\%$) albuminuria and proteinuria progression with an unbound plasma concentration EC_{50} of 32.0 nM (Supplemental figures 7 and 8). In this same study as a positive control, PF-06409577 was estimated to completely inhibit ($I_{max} = 100\%$) albuminuria and proteinuria progression with an unbound plasma concentration EC_{50} of 14.5 nM (supplemental figures 7 and 8).

All PK/PD analysis was conducted with NONMEM version 7.2 using first-order conditional estimation with interaction (FOCE I).

Table 1: PDE Selectivity Data for PF-249

PDE	IC₅₀ (nM)
PDE 11A4	>30000
PDE 6A	>30000
PDE 5A	>30000
PDE 4D3	70855
PDE 5A1	50578
PDE 3A1	37251
PDE 4D	>30000
PDE 8B	>30000
PDE 2A1	>30000
PDE 9A1	>30000
PDE 10A1	>30000
PDE 7B	>30000
PDE 3B	>30000
PDE 1B1	>30000

Table 2: CEREP Panel Selectivity Data for PF249

Target	Mode	Format	Endpoint (nM)	Compound PF-249
GPCR Targets				
Adenosine A1 (h)	Agonism	Impedance	EC ₅₀	>10000
Adenosine 2A (r)	Agonism	cAMP	EC ₅₀	>10000
Adrenergic Alpha 1A (h)	Agonism	[Ca ²⁺] _i	EC ₅₀	>10000
Adrenergic Alpha 1A (h)	Antagonism	[Ca ²⁺] _i	K _b	>10000
Adrenergic Alpha 2A (h)	Agonism	Impedance	EC ₅₀	>10000
Adrenergic Alpha 2B (h)	Agonism	cAMP	EC ₅₀	>10000
Adrenergic Alpha 2B (h)	Antagonism	cAMP	K _b	>10000
Adrenergic Beta 1 (h)	Agonism	cAMP	EC ₅₀	>10000
Adrenergic Beta 1 (h)	Antagonism	cAMP	K _b	>10000
Adrenergic Beta 2 (h)	Agonism	cAMP (β-Arrestin*)	EC ₅₀	>10000
Adrenergic Beta 2 (h)	Antagonism	cAMP (β-Arrestin*)	K _b	>10000
Angiotensin 1 (h)	Agonism	[Ca ²⁺] _i	EC ₅₀	>10000
Angiotensin 1 (h)	Antagonism	[Ca ²⁺] _i	K _b	>10000
Cannabinoid 1 (h)	Agonism	cAMP (β-Arrestin*)	EC ₅₀	>10000
Cannabinoid 1 (h)	Antagonism	cAMP (β-Arrestin*)	K _b	>10000
Cholecystokinin 2 (h)	Agonism	cAMP	EC ₅₀	>10000
Dopamine 1 (h)	Agonism	cAMP (*[Ca ²⁺] _i)	EC ₅₀	>10000
Dopamine 1 (h)	Antagonism	cAMP (*[Ca ²⁺] _i)	K _b	>10000
Dopamine 2S (h)	Agonism	Impedance	EC ₅₀	>10000
Dopamine 2S (h)	Antagonism	Impedance	K _b	>10000
Endothelin A (h)	Agonism	[Ca ²⁺] _i	EC ₅₀	>10000
Histamine 1 (h)	Agonism	[Ca ²⁺] _i	EC ₅₀	>10000
Histamine 1 (h)	Antagonism	[Ca ²⁺] _i	K _b	>10000
Histamine 2 (h)	Agonism	cAMP	EC ₅₀	>10000
Histamine 3 (h)	Agonism	cAMP	EC ₅₀	>10000
Neurokinin 1 (h)	Agonism	[Ca ²⁺] _i	EC ₅₀	>10000
Delta Opioid (m)	Agonism	Impedance	EC ₅₀	>10000
Kappa Opioid (r)	Agonism	cAMP	EC ₅₀	>10000
Mu Opioid (h)	Agonism	cAMP	EC ₅₀	>10000
Serotonin 1A (h)	Agonism	Impedance	EC ₅₀	>10000
Serotonin 1B (hm)	Agonism	Impedance	EC ₅₀	>10000
Serotonin 2A (h)	Agonism	IP1	EC ₅₀	>10000
Serotonin 2B (h)	Agonism	IP1	EC ₅₀	>10000
Serotonin 4E (h)	Agonism	cAMP	EC ₅₀	>10000
Vasopressin 1a (h)	Agonism	[Ca ²⁺] _i	EC ₅₀	>10000
NHR Targets				
Androgen Receptor (h)	Inhibition	Binding	K _i	>10000
Glucocorticoid Receptor (h)	Inhibition	Binding	K _i	>10000

Ion Channel Targets

Ca ²⁺ channel (DHP site) (r)	Inhibition	Binding	K _i	>10000
Ca ²⁺ channel (Diltiazem site) (r)	Inhibition	Binding	K _i	>10000
Ca ²⁺ channel (Verapamil site) (r)	Inhibition	Binding	K _i	>10000
Ca ²⁺ Cell Based Assay (r)	Inhibition	FLIPR (Ca ²⁺ Entry)	IC ₅₀	>10000
Na ⁺ channel (Site 2) (r)	Inhibition	Binding	K _i	>10000
Na ⁺ channel (Nav1.5) (h)	Inhibition	FLIPR (Membrane Potential)	IC ₅₀	>10000
Benzodiazepine Site (Central) (r)	Inhibition	Binding	K _i	>10000
Cl ⁻ channel (GABA-gated) (r)	Inhibition	Binding	K _i	3600
GABAA1 (α1,β2,γ2) (h)	Inhibition	Binding	K _i	>10000
AMPA Receptor (r)	Inhibition	Binding	K _i	>10000
NMDA Receptor (r)	Inhibition	Binding	K _i	>10000
Nicotinic (Neuronal α4β2) (h)	Inhibition	Binding	K _i	>10000
Nicotinic (Muscle-type) (h)	Inhibition	Binding	K _i	>10000
Phencyclidine Site (r)	Inhibition	Binding	K _i	>10000
Serotonin 3 (h)	Inhibition	Binding	K _i	>10000

Transporter Targets

Norepinephrine Trans. (NET) (h)	Inhibition	Binding (* Functional)	K _i	>10000
Dopamine Trans. (DAT) (h)	Inhibition	Binding (* Functional)	K _i	>10000
GABA Trans. (r)	Inhibition	Binding	K _i	>10000
Choline Trans. (CHT1) (h)	Inhibition	Binding	K _i	>10000
Serotonin Trans. (SERT) (h)	Inhibition	Binding (* Functional)	K _i	>10000

Enzyme/Kinase Targets

Cyclooxygenase 2 (h)	Inhibition	Enzyme	IC ₅₀	>10000
Phosphodiesterase 3B (h)	Inhibition	Enzyme	IC ₅₀	>10000
Phosphodiesterase 4D (h)	Inhibition	Enzyme	IC ₅₀	>10000
Angiotensin Converting Enzyme (h)	Inhibition	Enzyme	IC ₅₀	>10000
Acetylcholinesterase (h)	Inhibition	Enzyme	IC ₅₀	>10000
Monoamine Oxidase A (h)	Inhibition	Enzyme	IC ₅₀	>10000
Abl Kinase (h)	Inhibition	Kinase	IC ₅₀	>10000
EGFR Kinase (h)	Inhibition	Kinase	IC ₅₀	>10000
VEGFR2 Kinase (h)	Inhibition	Kinase	IC ₅₀	>10000
Lck Kinase (h)	Inhibition	Kinase	IC ₅₀	>10000
MAP Kinase 14 (p38α) (h)	Inhibition	Kinase	IC ₅₀	>10000
Src Kinase (h)	Inhibition	Kinase	IC ₅₀	>10000

* Indicates assay format used for profiling for specified compound. Target species include human (h), rat (r), hamster (hm) and mouse (m).

Abbreviations: GPCR, G-Protein Coupled Receptor; NHR, Nuclear Hormone Receptor; EGFR, Endothelial Growth Factor Receptor; VEGFR, Vascular Endothelial Growth Factor Kinase; Lck, Lymphocyte-Specific Protein Tyrosine Kinase; MAPK14, Mitogen Activated Protein Kinase 14 (p38α).

Table 3: Kinase Panel Selectivity Data for PF-249

Kinase	ATP Concentration	% Inhibition	PF-249 Concentration (μM)
PRKACA	ATP = Km	73.7	10
SRPK1	ATP = 50μM	37.0	10
AMPK	ATP = 50μM	36.0	10
JAK3	ATP = Km	35.5	10
NTRK1	ATP = Km	33.9	10
AURKA	ATP = Km	33.2	10
ACVRL1	Lantha Binding Assay	28.9	10
MAP3K9	ATP = 20μM	25.4	10
PIP4K2A	ATP = 10μM	20.9	10
STK39	Lantha Binding Assay	19.9	10
DYRK2	ATP = 50μM	17.7	10
PRKACA	ATP = Km	17.4	1
CDK2_CyclinA	ATP = Km	17.1	10
MYLK	ATP = 50μM	16.2	10
GSK3B	ATP = Km	12.7	10
IRAK4	ATP = 1000μM	12.1	10
CSK	ATP = 20μM	11.5	10
AKT2	ATP = 50μM	11.3	10
KIT	1 mM ATP	11.1	10
ROCK1	ATP = 1000μM	10.9	10
CSNK2A2	ATP = Km	10.5	10
PLK1	ATP = 5μM	10.4	10
PIK3CA	ATP = 10μM	10.4	10
TEK	ATP = Km	10.4	10
MAPK15	ATP = 5μM	9.8	10
PRKCB2	ATP = Km	9.8	10
MINK1	ATP = Km	9.8	10
LCK	ATP = Km	9.1	10
TNIK	ATP = Km	8.5	10
NUAK1	ATP = 20μM	8.4	10
DYRK3	ATP = Km	8.4	10
CAMK2A	ATP = Km	7.7	10
MAP3K11	ATP = 20μM	7.7	10
MAPK8	ATP = Km	7.5	10
STK3	ATP = Km	7.2	10
MAPK8	ATP = 20μM	6.8	10
SGK1	ATP = 1000μM	6.7	10
MET	ATP = Km	6.3	10
ROCK1	ATP = Km	6.2	10

CAMK1	ATP = 50μM	6.2	10
MYLK2	ATP = 1000μM	6.1	10
ABL1	ATP = Km	6.0	10
MKK1	ATP = 5μM	5.9	10
NEK6	ATP = 50μM	5.9	10
LCK	ATP = Km	5.8	10
KDR	ATP = Km	5.6	10
PIM3	ATP = 20μM	5.5	10
PRKD1	ATP = 50μM	5.5	10
AURKA	ATP = Km	5.5	10
INSR	ATP = Km	5.4	10
PDPK1	ATP = Km	5.3	10
LCK	ATP = Km	5.3	1
MARK1	ATP = Km	4.8	10
JAK2	ATP = Km	4.5	1
EPHA2	ATP = Km	4.4	10
JAK2	ATP = Km	4.1	10
	Lantha Binding		
MYLK3	Assay	4.1	10
Rock2	ATP = 20μM	4.0	10
PIM1	ATP = 20μM	4.0	10
Rps6ka1	ATP = 50μM	3.8	10
TNIK	ATP = Km	3.8	1
BTK	ATP = Km	3.7	10
FGFR1	ATP = Km	3.7	10
PDPK1	ATP = Km	3.5	1
CSNK1A1	ATP = Km	3.3	10
KDR	ATP = Km	3.3	10
	Lantha Binding		
MYLK	Assay	3.2	10
MAP4K4	ATP = Km	3.2	10
SRC	ATP = Km	3.1	10
IGF1R	1 mM ATP	3.0	10
p38	ATP = Km	3.0	1
Csnk1d	ATP = 20μM	2.8	10
MAPKAPK2	ATP = Km	2.7	1
AKT1	ATP = Km	2.7	10
FGFR1	ATP = Km	2.7	1
MST4	ATP = Km	2.4	1
SRC	ATP = Km	2.1	10
NEK2	ATP = Km	1.9	10
FGR	1 mM ATP	1.6	10
TTK	ATP = 20μM	1.5	10
KDR	ATP = 1000μM	1.5	10

MAP4K4	ATP = Km	1.5	1
MYLK2	ATP = Km	1.4	10
MAPKAPK2	ATP = Km	1.4	10
MINK1	ATP = Km	1.4	1
ABL1	ATP = Km	1.0	1
MAPKAPK5	ATP = 20μM	1.0	10
CDK2_CyclinA	ATP = Km	0.9	1
SRC	ATP = Km	0.8	1
PI4KB	ATP = 10μM	0.7	10
CHEK2	ATP = Km	0.6	10
CSNK1A1L	ATP = Km	0.4	10
SPHK1	ATP = 10μM	0.4	10
ABL1	ATP = Km	0.2	10
MAPK8	ATP = Km	0.2	1
p38	ATP = Km	-0.3	10
EPHA2	ATP = Km	-0.3	10
CDK2_CyclinA	ATP = Km	-0.5	10
PDPK1	ATP = Km	-0.6	10
SGK1	ATP = Km	-0.7	10
IRAK4	ATP = Km	-1.0	10
PBK	ATP = 50μM	-1.0	10
GSK3B	ATP = Km	-1.0	10
MARK3	ATP = 5μM	-1.0	10
TAOK2	ATP = Km	-1.1	10
CSNK1A1L	ATP = Km	-1.3	1
KDR	ATP = Km	-1.3	1
MAP4K2	ATP = 20μM	-1.4	10
MAPK14	ATP = Km	-1.4	10
CHEK1	ATP = Km	-1.4	10
DYRK3	ATP = Km	-1.4	1
MAPKAPK2	ATP = Km	-1.5	10
MAPK1	ATP = Km	-1.8	10
GSK3B	ATP = Km	-1.8	1
CHKA	ATP = 1μM	-2.0	10
PRKACA	ATP = Km	-2.0	10
EGFR	ATP = Km	-2.1	10
PRKACA	1 mM ATP	-2.3	10
PIM2	ATP = Km	-2.3	10
MAPK1	ATP = 1000μM	-2.7	10
EGFR	ATP = 1000μM	-2.7	10
TEK	ATP = 1000μM	-2.7	10
CAMK2A	ATP = Km	-2.8	10
JAK2	1 mM ATP	-3.0	10
CHEK1	ATP = Km	-3.0	1

PAK4	ATP = Km	-3.0	10
PIK3CB	ATP = 10 μ M	-3.5	10
EPHA2	ATP = Km	-3.5	1
PKN2	ATP = 5 μ M	-3.6	10
TAOK2	ATP = Km	-4.0	1
MST4	ATP = Km	-4.3	10
NTRK1	ATP = 20 μ M	-4.5	10
AURKA	ATP = Km	-4.9	1
FLT1	1 mM ATP	-5.0	10
CHEK1	ATP = Km	-5.2	10
CSK	1 mM ATP	-5.4	10
RPS6KA3	ATP = 50 μ M	-5.6	10
TAOK2	ATP = Km	-5.6	10
MAP4K4	ATP = Km	-5.7	10
ERBB4	ATP = 5 μ M	-6.5	10
INSR	1 mM ATP	-7.6	10
PRKCA	ATP = 20 μ M	-7.8	10
RPS6KA5	ATP = 20 μ M	-7.9	10
AURKB	ATP = 20 μ M	-8.1	10
CAMK2A	ATP = Km	-8.5	1
MAPK13	ATP = 5 μ M	-8.7	10
FGFR1	ATP = Km	-8.7	10
MST4	ATP = Km	-9.5	10
MAPK12	ATP = 5 μ M	-9.6	10
Lck	ATP = 50 μ M	-10.0	10
MINK1	ATP = 50 μ M	-10.3	10
Dyrk1a	ATP = 50 μ M	-10.8	10
MKNK2	ATP = 50 μ M	-11.0	10
AKT1	ATP = 5 μ M	-11.1	10
CSNK2A1	ATP = 5 μ M	-11.1	10
RPS6KB1	ATP = 20 μ M	-11.2	10
MAPK3	1 mM ATP	-11.5	10
IRAK4	ATP = 20 μ M	-12.1	10
PI4KA	ATP = 10 μ M	-12.3	10
EEF2K	ATP = 5 μ M	-12.4	10
CAMKK2	ATP = 20 μ M	-12.4	10
MKNK1	ATP = 50 μ M	-14.7	10
MAP3K7	ATP = 5 μ M	-15.2	10
STK11	ATP = 20 μ M	-21.0	10
SPHK2	ATP = 1 μ M	-21.1	10
IKBKB	ATP = 5 μ M	-21.1	10
DGKB	ATP = 10 μ M	-23.4	10
MAPK9	ATP = 20 μ M	-27.6	10
PIK3CG	ATP = 10 μ M	-42.1	10

TABLE 4

Summary of Pharmacokinetics of PF-06409577 and PF-249 in Wistar-Han Rats

Compound	Route	Dose (mg/kg)	CL _p (mL/min/kg)	V _{dss} (L/kg)	t _{1/2} (h)	C _{max} (ng/mL)	T _{max} (h) ^b	AUC ₍₀₋₂₄₎ (ng.h/mL)	Oral F (%) ^b
PF-06409577	i.v.	1.0 (n=3)	22.6 ± 3.05	0.84 ± 0.53	1.06 ± 0.8	N.A.	N.A.	744 ± 103	
	p.o.	3.0 (n=3)	N.A.	N.A.	N.A.	110 ± 71.9	0.33 ± 0.14	329 ± 57.0	15.0
	p.o.	10 (n=3)	N.A.	N.A.	N.A.	1900 ± 464	0.33 ± 0.14	1880 ± 258	25.0
	p.o.	30 (n=3)	N.A.	N.A.	N.A.	4020 ± 1860	0.5 ± 0.0	10500 ± 1910	47.0
PF-249	i.v.	0.5 (n=2)	0.05 (0.038,0.061)	0.104 (0.097,0.11)	27.2 (31.7,22.7)	N.A.	N.A.	254000 (296000,212000)	
	p.o.	3.0 (n=2)	N.A.	N.A.	N.A.	10200 (8420,11900)	5.5 (7.0,4.0)	160000 (136000,184000)	52

TABLE 5. Summary pharmacokinetics of PF-06409577 dose response study

Dose (mg/kg)	$C_{average}$ (nM free)	C_{max} (nM free)	AUC (nM·h free)
10	1.36	4.07	32.7
30	4.59	13.7	110
100	22.2	66.2	533

Table 6. Summary pharmacokinetics from PF-249 ZSF-1 dose response study.

Dose (mg/kg)	$C_{average}$ (nM free)	C_{max} (nM free)	AUC (nM·h free)
3	17.4	18.6	417
10	20.2	21.7	485
30	50.3	54.0	1210

TABLE 7

Summary of ZSF-1 Rat Urine Endpoints Prior to Initiation of Treatment in the PF-249 Dose Response Study

Treatment	Dose (mg/kg)	Urine Volume (mL)	Urinary Urea Nitrogen (mg/dL)	Urine Creatinine (mg/dL)
Lean Vehicle	0	5.83 ± 0.59****	3413 ± 189.06***	102.13 ± 6.89****
Obese Vehicle	0	42.83 ± 5.19	2273 ± 220.76	34.48 ± 3.70
PF-249	3	41.25 ± 4.04	2250 ± 175.25	34.10 ± 3.15
	10	38.17 ± 4.46	2300 ± 194.33	35.17 ± 2.91
	30	39.33 ± 3.85	2378 ± 233.79	35.17 ± 3.52
PF-06409577	100	39.33 ± 4.70	2278 ± 171.79	34.28 ± 2.90
Ramipril	1	43.33 ± 4.58	2173 ± 185.92	33.19 ± 2.88

Supplemental Figure Legends**Supplemental Figure 1**

A. Kinetic studies of AMPK in the presence of PF-06409577 and PF-249 at varied substrate peptide concentrations. B-D. Impact of (B) PF-06409577, (C) AMP, or (D) PF-249 on the protection of AMPK phosphorylation in the presence of protein phosphatase.

Supplemental Figure 2

Kidney pAMPK/tAMPK ratio in wistar han rats in the presence of the indicated oral dose of PF-249. Tissues were collected 1 hour after compound dosing and phospho and total AMPK measured by quantitative ELISA.

Supplemental Figure 3

Representative renal histopathology from PF-06409577 study **A**. (A) Lean control animal with no significant abnormalities in the kidney; (B) Obese animal demonstrating protein casts in renal tubules (arrow). and glomerular defects (C) Obese animal treated with PF-06409577. The presence of protein casts is reduced but no dramatic impact on glomerular improvement is noted; there is increased vacuolation of thick ascending limb epithelium (arrow). H&E stain. Bar = 200 microns. (D) Transmission electron micrograph of glomeruli from lean animals demonstrating normal podocyte (P) foot processes; (E) Obese animal showing podocyte foot process fusion; (F) PF-577 treated animals showing similar podocyte foot process fusion as was seen in obese animals. Bar = 1mciron.

Supplemental Figure 4

PK/PD model of ZSF1 rat albuminuria and proteinuria disease progression inhibition by AMPK activators PF-06409577 and PF-249

Supplemental Figure 5

PF-06409577 inhibition of ZSF1 rat proteinuria and albuminuria disease progression PK/PD model

Supplemental Figure 6

PF-06409577 oral exposure profiles in ZSF1 rat in the PF-06409577 dose response study

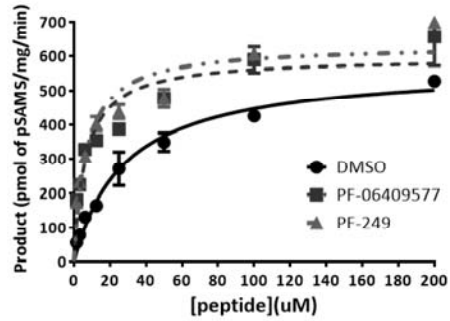
Supplemental Figure 7

PF-249 and PF-06409577 inhibition of ZSF1 rat proteinuria and albuminuria disease progression PK/PD model.

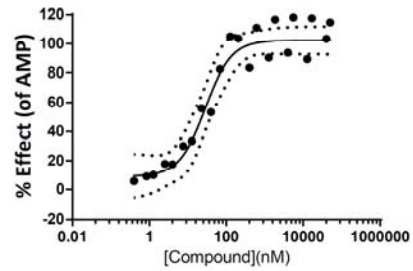
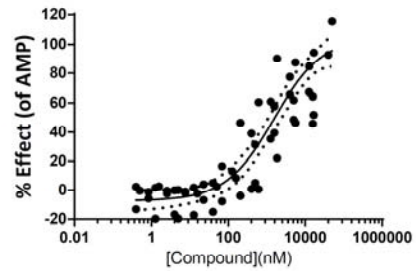
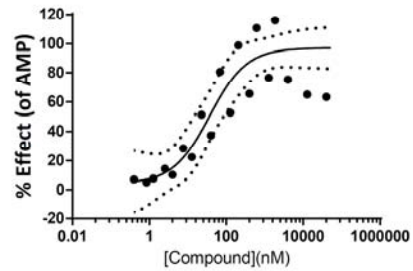
Supplemental Figure 8

PF-249 and PF-06409577 oral exposure profiles in the ZSF1 rat in the PF-249 dose response study

Supplemental Figure 1

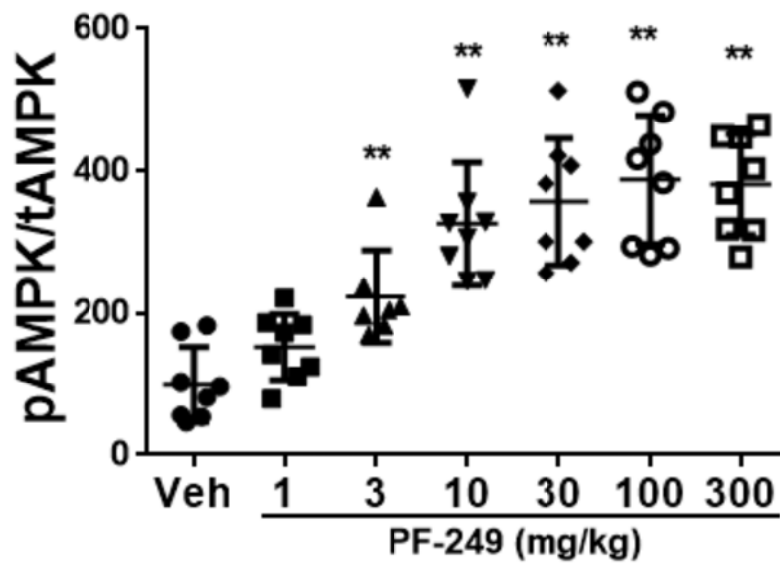
A

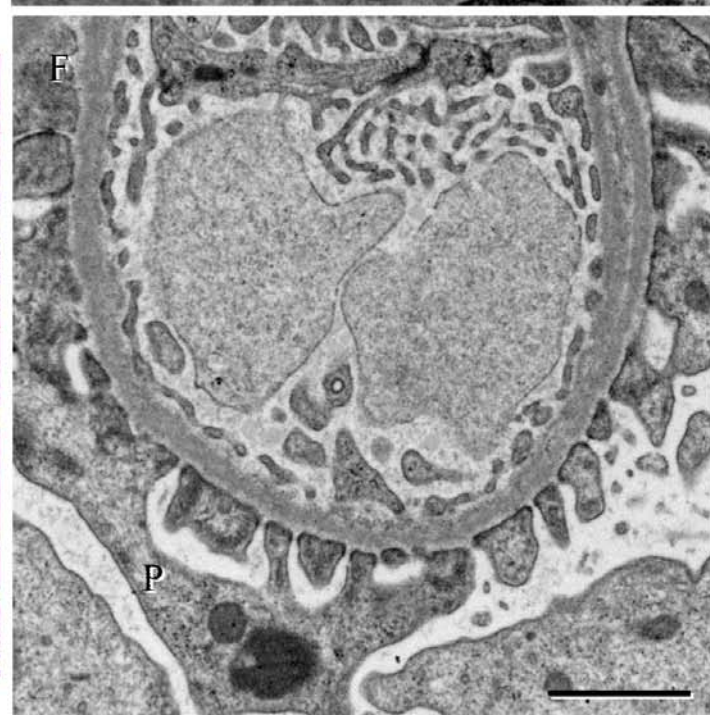
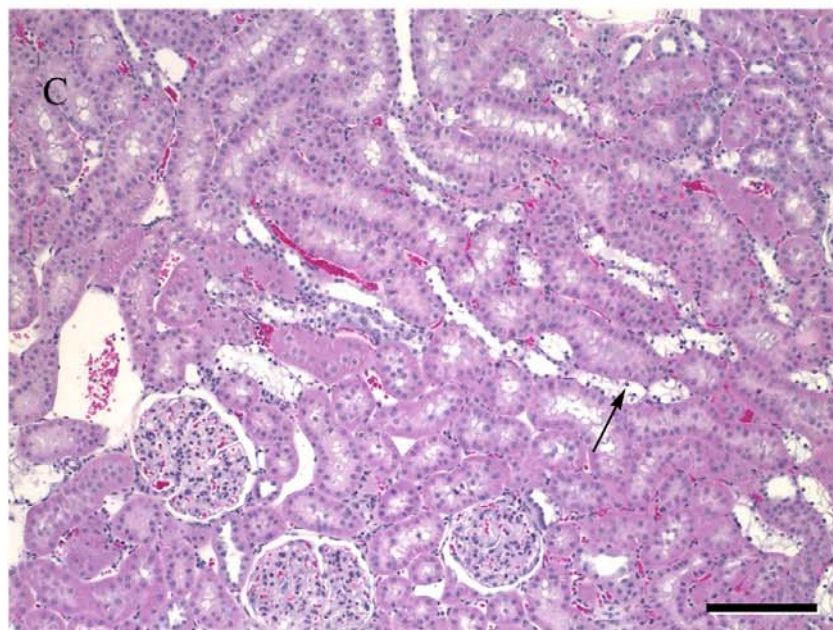
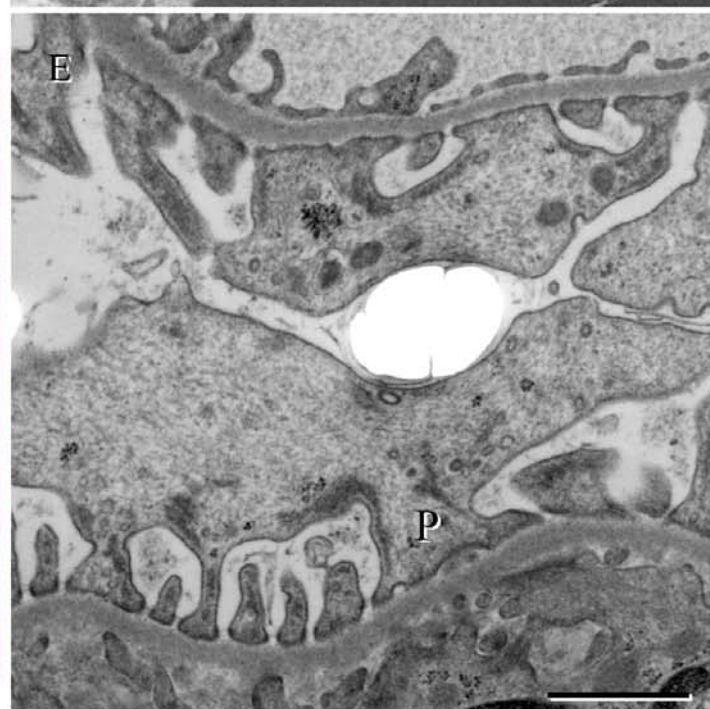
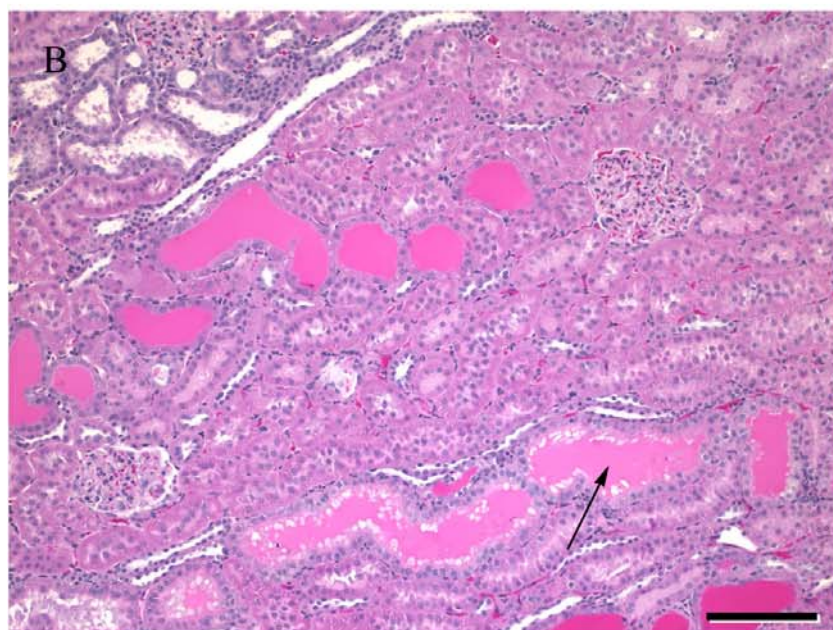
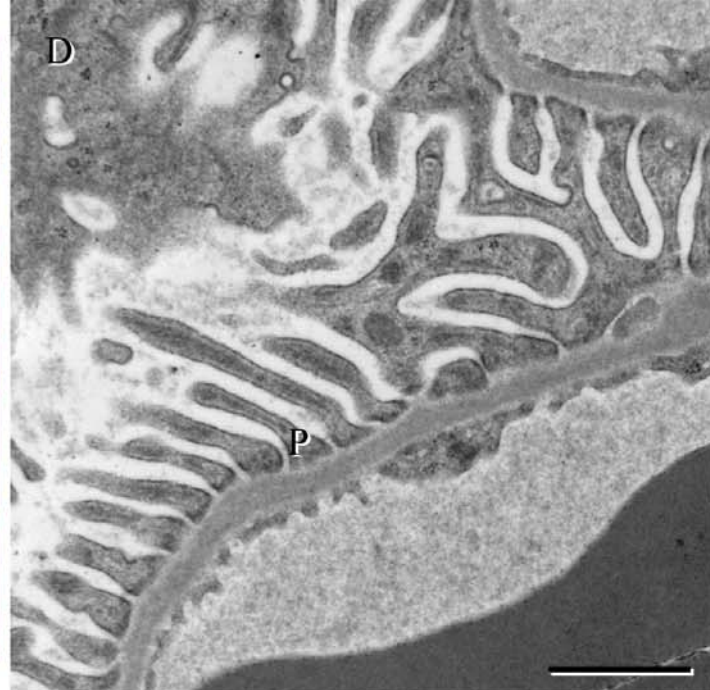
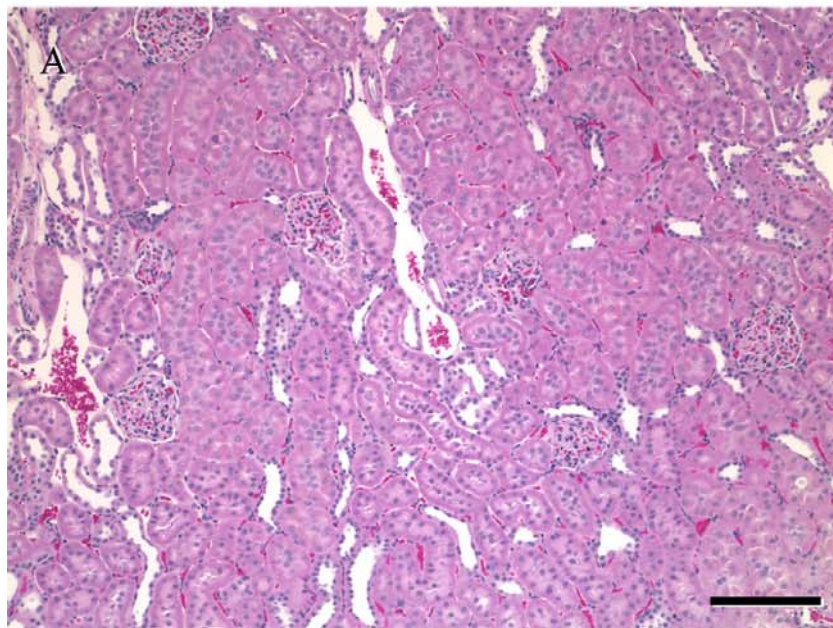
	K_m ($\mu\text{mol/L}$ of peptide)	V_{max} pmol of pSAMS/mg/min
DMSO	28.07 ± 4.11	572.7 ± 27.7
10 μM PF-06409577	6.387 ± 1.55	596.6 ± 34.3
10 μM PF-249	6.692 ± 1.29	631.5 ± 29.1

BPF-06409577 Protection only
n=3**C**AMP Protection only
n=9**D**PF-249 Protection only
n=2

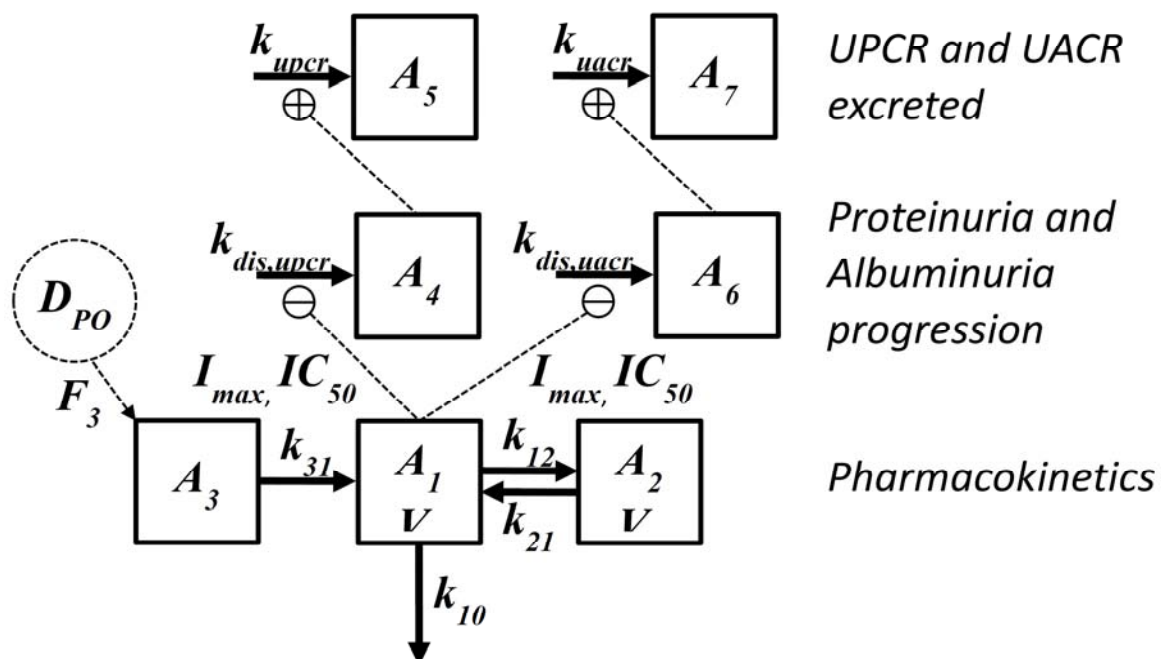
Supplemental Figure 2

A

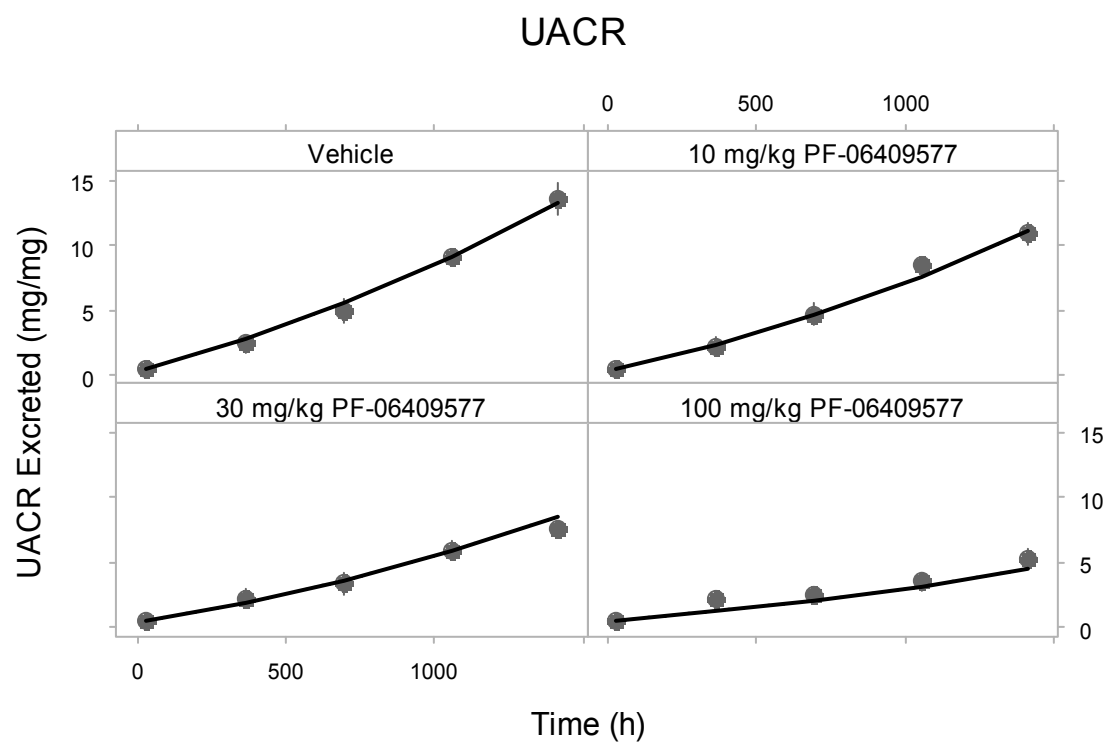
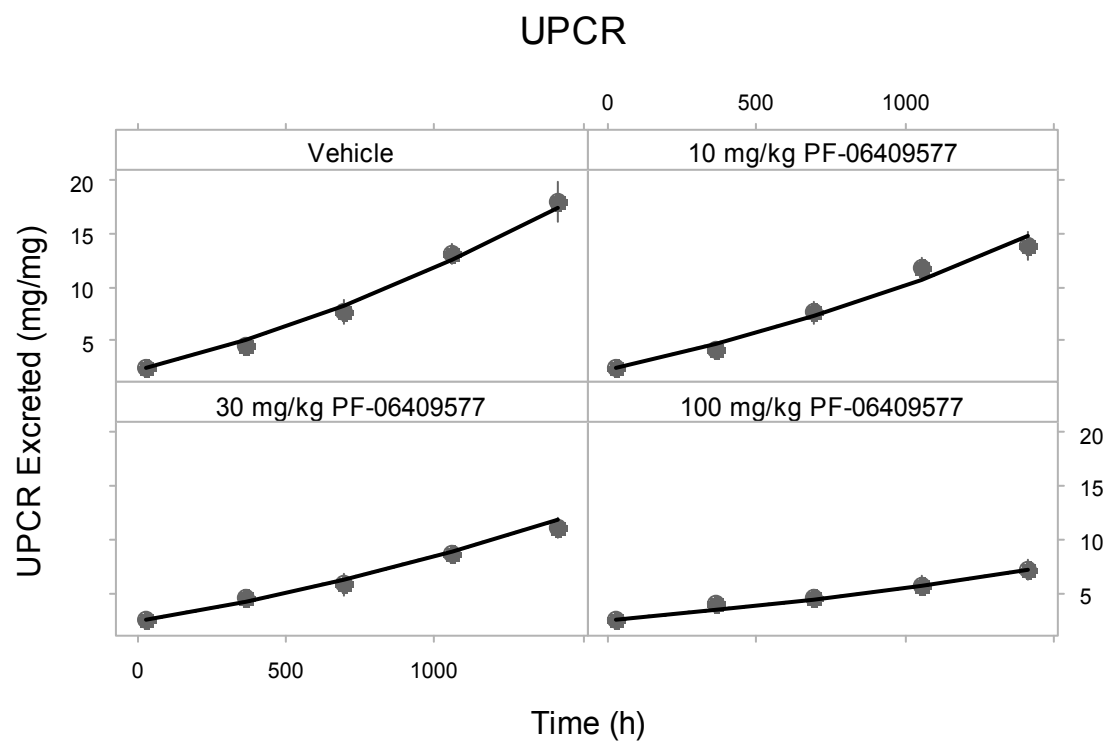




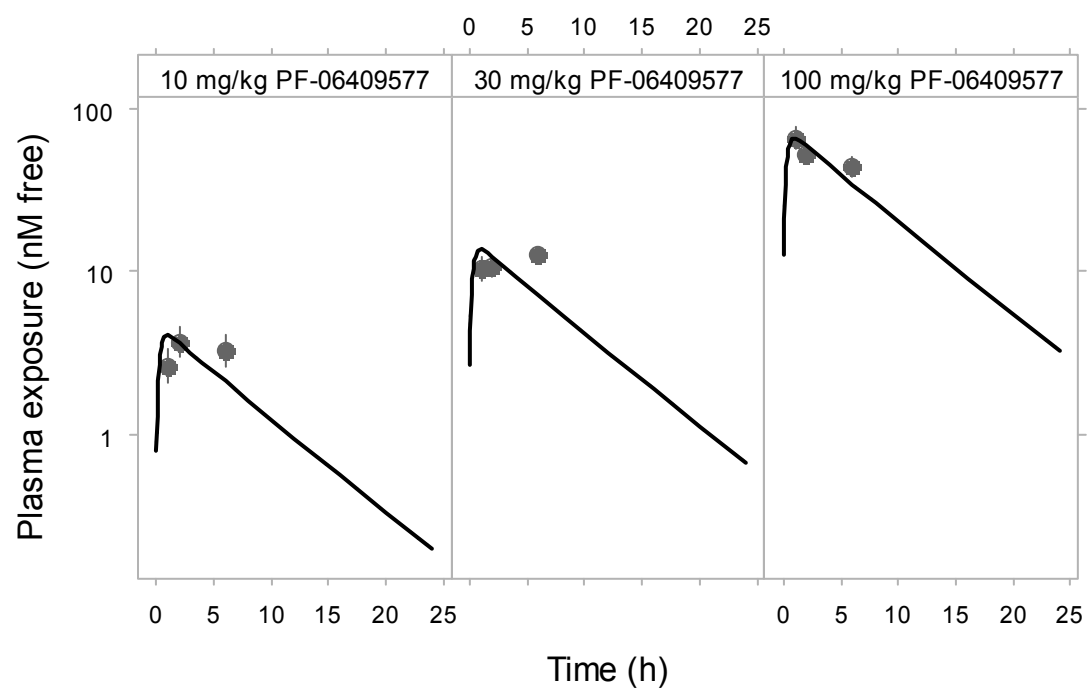
Supplemental Figure 4



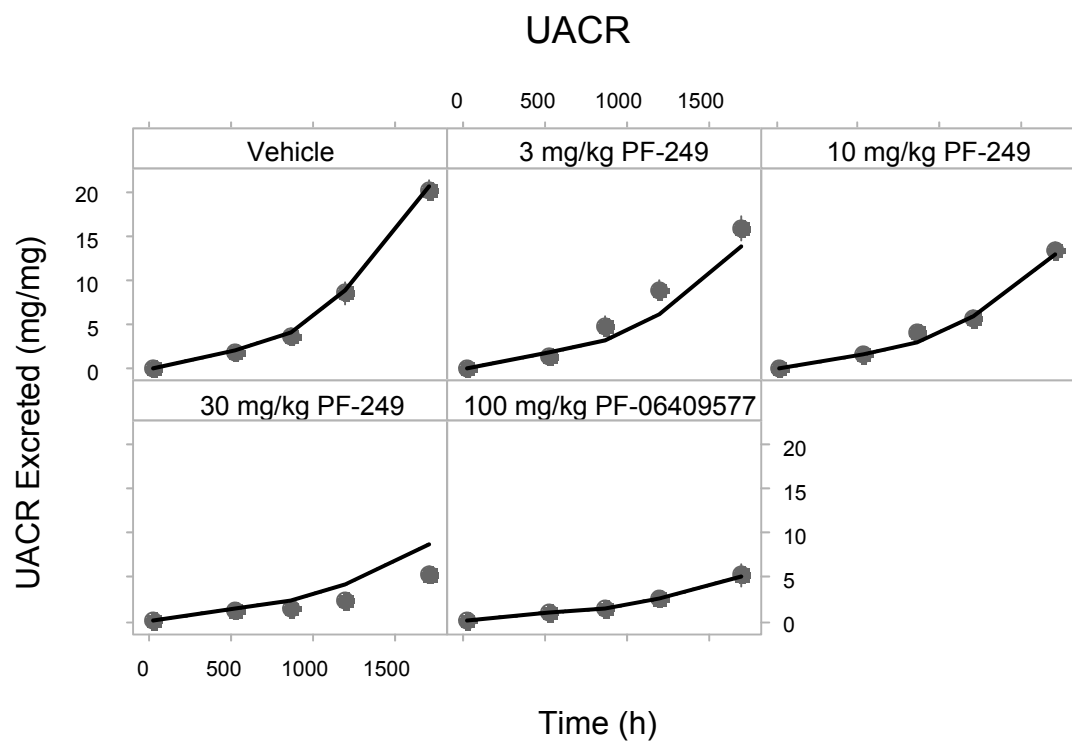
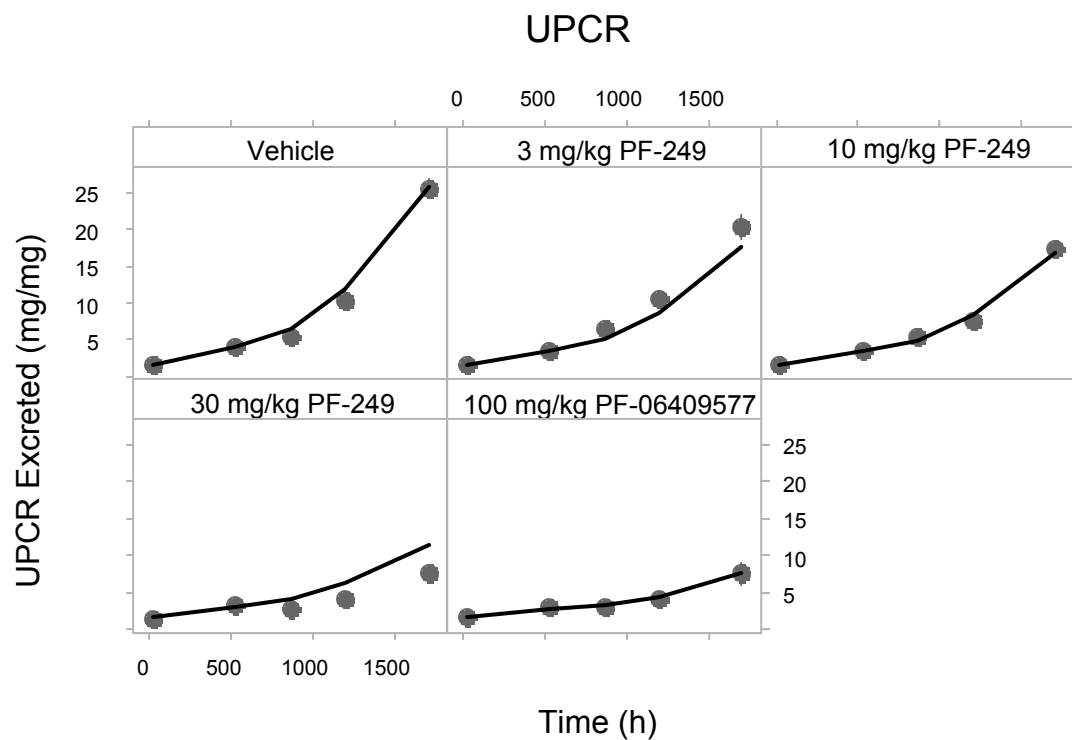
Supplemental Figure 5



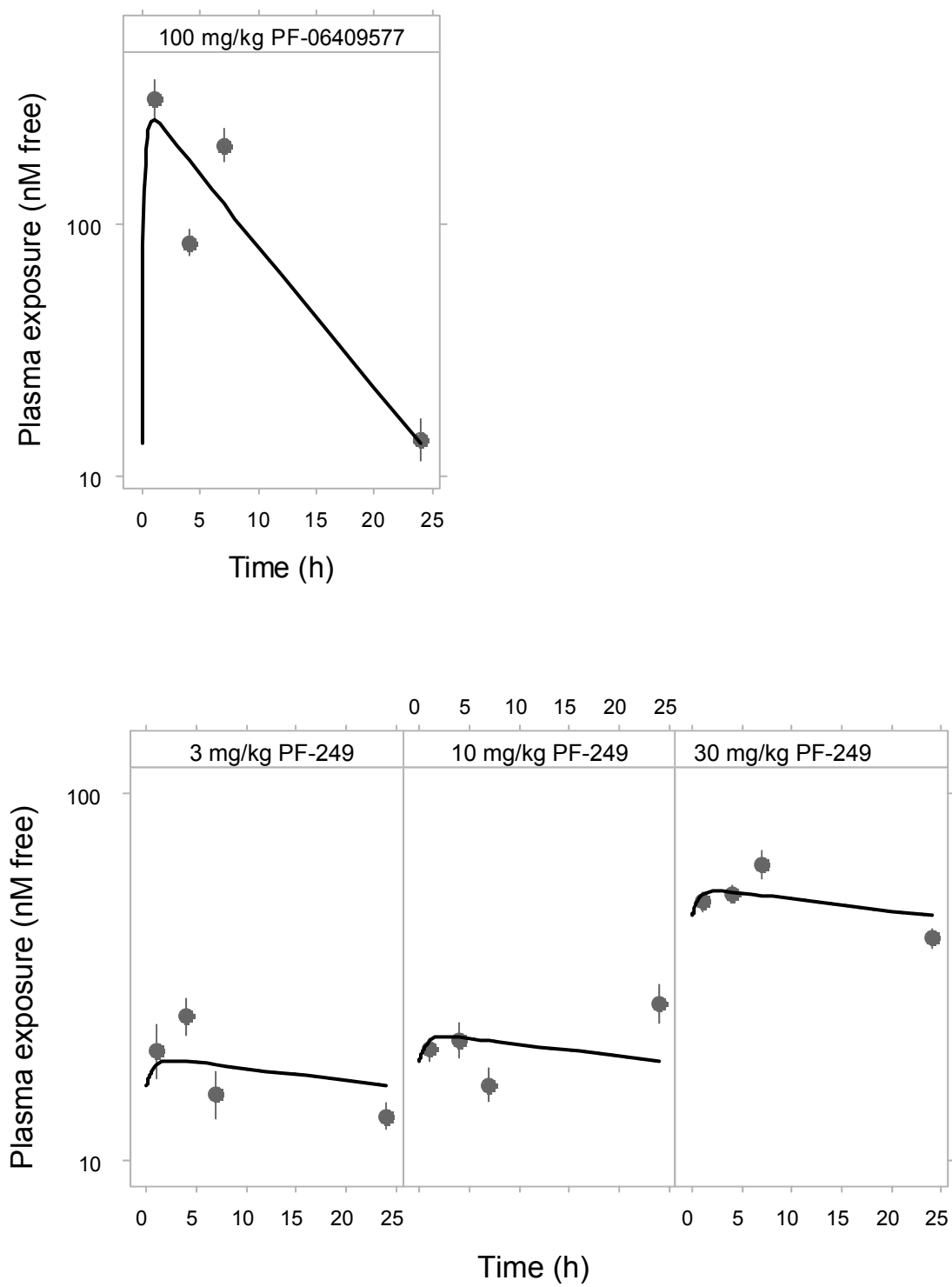
Supplemental Figure 6



Supplemental Figure 7



Supplemental Figure 8



Supplemental References

1. Cameron KO, Kung DW, Kalgutkar AS, Kurumbail RG, Miller R, Salatto CT, Ward J, Withka JM, Bhattacharya SK, Boehm M, et al. Discovery and Preclinical Characterization of 6-Chloro-5-[4-(1-hydroxycyclobutyl)phenyl]-1H-indole-3-carboxylic Acid (PF-06409577), a Direct Activator of Adenosine Monophosphate-activated Protein Kinase (AMPK), for the Potential Treatment of Diabetic Nephropathy. *J Med Chem*. 2016;59(17):8068-81.
2. Calabrese MF, Rajamohan F, Harris MS, Caspers NL, Magyar R, Withka JM, Wang H, Borzilleri KA, Sahasrabudhe PV, Hoth LR, et al. Structural basis for AMPK activation: natural and synthetic ligands regulate kinase activity from opposite poles by different molecular mechanisms. *Structure*. 2014;22(8):1161-72.
3. Ikehara T, Shinjo F, Ikehara S, Imamura S, and Yasumoto T. Baculovirus expression, purification, and characterization of human protein phosphatase 2A catalytic subunits alpha and beta. *Protein Expr Purif*. 2006;45(1):150-6.